eISSN: 2791-8742
doi: 10.52460/src

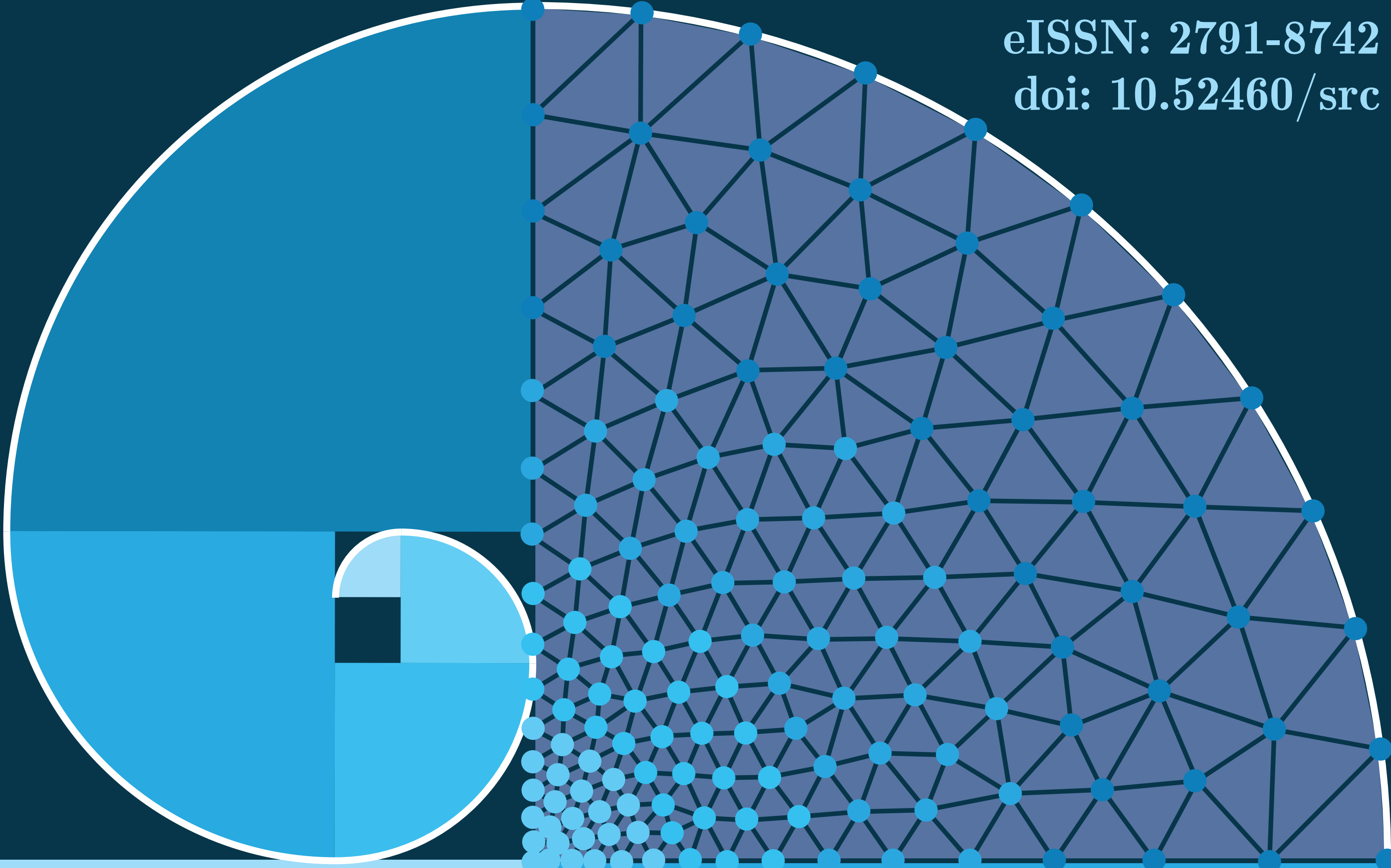

Scientific Research Communications

Volume 2
Issue 1
January 2022

Scientific Research Communications
Volume 2, Issue 1, 2022

Editorial

Publisher
Prof. Dr. Mehmet ÇEVİK
İzmir International Guest Students Association

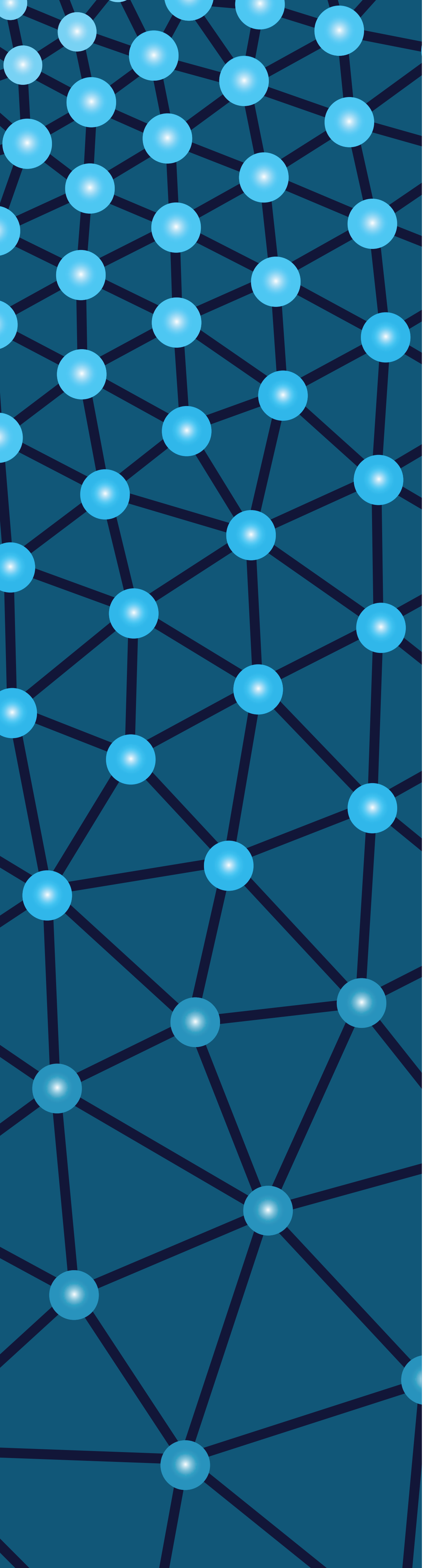

Scientific Research Communications
Volume 2, Issue 1, 2022

Contents

Research Articles

Scientific Research Communications

Research Article
Sci. Res. Comm. (2022)
Volume 2, Issue 1
doi: 10.52460/src.2022.001

Recovery of Pressed Titanium Alloy Machining Chip via Vacuum Induction Melting

Erdoğan Teke[1,*], Mücahit Sütçü[2], Yıldıray Başkurt[3], M. Özgür Seydibeyoğlu[2,4]

[1] Graduate School of Natural and Applied Science, İzmir Kâtip Çelebi University, Turkey
[2] Department of Materials Science and Engineering, İzmir Kâtip Çelebi University, Turkey
[3] Department of Electrical and Electronics Engineering, Dokuz Eylül University, Turkey
[4]Advanced Structures & Composites Center, University of Maine, USA
*Corresponding author: erdoganteke@gmail.com

Received: 25.09.2021 Accepted: 27.01.2022

Abstract

Among many precious metals, titanium has been the first priority in various applications such as aerospace, automotive, marine and medical sectors due its superior mechanical, electrochemical, and biocompatible properties. In this study, a new melting method with vacuum induction system for Ti6Al4V alloy was developed to recover titanium scraps that were collected from medical implant machining industry. Prior to melting processing the recovered material was cleaned with ethyl alcohol and acetone (96% purity) to remove the coolant oil in the metal scraps. After the melting process, the microstructure, phase and hardness properties of melted bulk specimen were investigated by SEM, EDS, optical microscopy, XRD analysis and Rockwell hardness test. The results reveal that despite the high oxygen content, these molten bulk materials can be used in engineering applications other than biomaterials.

Keywords: Vacuum induction melting (VIM); titanium; waste scraps; recycling; microstructure.

1. Introduction

Titanium and its alloys are extensively used in many industries such as aerospace, biomedical, marine and automotive because of their good mechanical, physical and chemical properties (Froes, 2013), (Destefani, 1990), (Leyens & Peters, 2003). The main advantages of titanium is its high strength-to-weight ratio and corrosion resistance. Its tensile and flexural strengths are comparable to steel, but the density is just the half of it (Leyens & Peters, 2003), (Donachie, 2000). The most common used titanium alloy is Ti6Al4V, an α+β alloy, and has high toughness and working temperature, low density, excellent corrosion resistance and biological inertness it (Facchini et al., 2009), (Rack & Qazi, 2006).

The most common manufacturing process of titanium-based products is usually computer numerical control (CNC) machining. In industrial production processes, the crucial waste titanium scraps are emerged after machining processes of its rods. The amount of scraps corresponds to 40% of the starting material used in the manufacturing of Ti6Al4V parts, and in some cases, much higher. These machining scraps are generally either collected in containers for recycling, or thrown into the waste storage area due to the risk of self-ignition. Disposed of Ti6Al4V alloy waste, which is in the category of precious materials, creates both environmental and economic problems (Dikici & Sutcu, 2017).

After machining, titanium scrap is generated in the forms of solid, turning and chip that result in the processing of bars, sheets, forge flashings, welding. The turnings usually contain some cutting lubricants; these wastes may also be contaminated with oil or grease (Neff, 1990). In recycling processes, the removal of these metal scrap from lubricant impurities is an important surface cleaning process. These pretreatments directly affect the quality of the materials to be produced in the recycling methods to be applied. Therefore, surface cleaning operations of scrap are important which can be costly and difficult.

In recent years, more than one manufacturing techniques such as melting and powder metallurgy processing for the recycling of precious metals such as titanium have been studied. In industrial applications, melting is generally a preferred method. Different melting methods such as vacuum arc re-melting (VAR) and electron beam melting (EBM) are available for the recovery of titanium scrap by melting. The melting of titanium alloys is carried out in common vacuum or an inert atmosphere vacuum (typically argon) (ASM Handbook, 2008). For the recycling of titanium and its alloys, it is important to note that titanium has a high affinity for oxygen and nitrogen (Topolski et al., 2017). Recently, some researches on the recycling of the titanium scraps with different methods were done by the researchers. Moon et al.(2017) focused on recycling of titanium scrap via the electromagnetic cold crucible (EMCC) technique (Moon et al., 2017). The scraps were successfully refined by this technique. Oh, & Lim (2016) used vacuum arc-remelting (VAR) process to melt pure Ti and Ti alloys scraps in inert atmosphere (Ar-H_2) (Oh, & Lim, 2016). They investigated the effect of hydrogen-plasma arc melting (HPAM) on the removal of metallic and gaseous impurities from pure titanium and titanium alloys. Su et al. (2009) studied the effect of hydrogen on the oxygen content of Ti6Al4V alloy through the remelting route in electric arc furnace (Su et al., 2009). Vutova et al. (2010) performed Ti from waste products by electron beam melting. The working vacuum pressure was $5–8\times10^{-3}$ Pa (Vutova et al., 2010). Roh et al. (2014) produced low oxygen content TiNi alloy powder from TiNi alloy scraps by using vacuum arc-remelting process (Roh et al., 2014). Ahmed et al. (2017) focused on the production of well-finished part made of Ti6Al4V from the powder by EBM (Ahmet et al., 2017).

Induction heating is the process of heating an electrically conducting part by passing an alternate current at a specific frequency through a copper coil to generate a variable electromagnetic field, which generates induced eddy currents in the vicinity of the coil. The eddy currents flowing through the part's resistance, which is placed within the coil, heat it via the Joule effect. These eddy currents are caused by the part's resistance and result in power loss. This power loss manifests itself as heat. The vacuum induction melting process exhibits several advantages: low cost, short melting time, homogeneous mixing, precise control of the temperature, easily accessible and being energy efficient (Sazak, 1999), (Rudnev et al., 2003).

In this study, a new melting system with vacuum induction for Ti6Al4V alloy was developed to recover the titanium chip that was collected from medical implant machining industry. After the vacuum induction melting process, the physical, microstructural and mechanical properties of the melted bulk Ti6Al4V sample was investigated.

2. Materials and method

2.1. Preparation of Ti6Al4V alloy chip

Ti6Al4V alloy scraps were used as the initial materials in this study in the chip form obtained by CNC machining. Chip cleaning is also one of the main factors that determines the quality of melt material. High level of contamination with foreign particles will affect the elemental composition. During machining, the surface of the titanium chip is contaminated with lubricating, cooling oil or oxide. Prior to melting processing, the titanium scraps were cleaned with detergent and ethyl alcohol (96% purity) to remove the coolant oil. The Ti6Al4V scraps were crushed in chips form under 5 mm to reduce the size by mechanical crusher. Then, the reduced size chip was compressed into a cylindrical briquette by applying 170 tons pressing in a hydraulic press. The Ti6Al4V scraps in the form of chips and briquettes prepared before melting are given in Figure 1. The Ti6Al4V alloy has low thermal and electrical conductivity. In order to make a quick and easy melting process, the pores or voids inside the briquettes must be at a minimum level. For this reason, reducing the size of the chip facilitates both the pressing process and the formation of briquettes with less pores.

Figure 1. (a) The Ti6Al4V chip and (b) the briquettes pressed from their chip

2.2. Vacuum induction melting (VIM) system

The melting process was performed within a low pressure chamber equipped with a water-cooled induction coil, as it is given schematically in Figure 2. Here, the induction coil was operated with a medium frequency power supply.

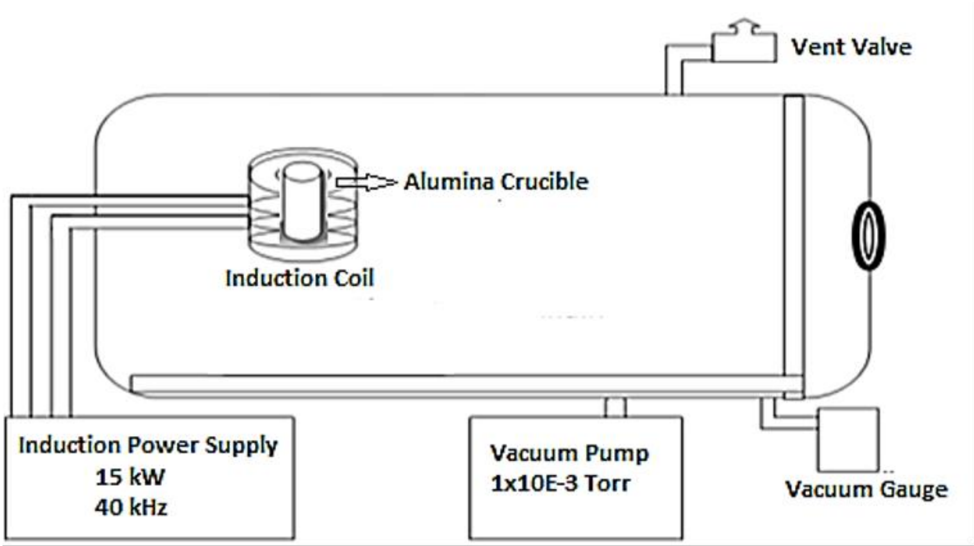

Figure 2. The vacuum induction melting (VIM) system

Prior to melting process, the base pressure of the system was maintained at 1×10^{-3} torr for 30 minutes to minimize the presence of foreign particles in the environment. The vacuum value of the system, the applied power and the crucible material are important parameters affecting the mechanical and chemical properties of the obtained sample. The melting process was carried out at pressure of $2{,}1\times10^{-2}$ torr due to the resulting heat. Alumina crucible with 99,8% purity was used because of its resistance to oxidation at high temperatures. The induction power was applied gradually to prevent the crucible from being affected by thermal shocks. A medium frequency induction generator with a power of 15 kW was specially produced for the melting process. One of the most basic parameters of the generator design is to determine the operating frequency. Alternating currents can flow efficiently from the surface to a certain depth depending on their frequencies, the magnetic and electrical properties of the conductor through which they pass. However, the chip was pressed under high pressure and turned into briquettes. Thus, the pressed compacts are not in the form of a uniform structure and they don't have a uniform structure of completely discrete particles. Each chip particle touches one another mechanically but is not in absolute contact with possible oxidation and pollution causes. The application frequency with these assumptions was chosen empirically in the order of 40 kHz. During the melting process, the operating frequency was measured as 39.67 kHz. After melting, the specimen was allowed to cool in vacuum for 1 hour.

For microstructural investigation, the specimen was cut with diamond disc and then its surface were grinded with silicon carbide (SiC) grinding papers of 180-320-600-1200 grit, respectively. Then, the VIM molten Ti6Al4V sample surfaces were polished with diamond solutions of 9-3-1 µm, respectively. To reveal the microstructure of polished surface, chemical etching on the sample surface was carried out using an etchant solution composed of 10 ml of hydrofluoric acid (HF), 5 ml nitric acid (HNO_3), and 85 ml of water.

2.3. Characterization

The phase analysis of the VIM molten Ti6Al4V sample was carried out using a Bruker Phaser D2 diffractometer with a Cu-Kα x-ray (λ= 1.5404 Å; 30 kV) diffraction beam.

The elemental analysis and morphology of VIM molten Ti6Al4V sample and chip were investigated by using SEM-EDS, by Carl Zeiss 300VP scanning electron microscopy with Energy Dispersive Spectrometry (EDS). The crystalline phase formations and microstructure of the VIM molten Ti6Al4V were examined by optical microscope (OM) by using Nikon Eclipse LV150N. HRC hardness tests preloading at 98 N and max. loading at 1471 N in 3 seconds were conducted at room temperature using a Prüfen+Messen Tester machine. The density of the VIM molten Ti6Al4V sample was determined using Archimedean method at room temperature. The surface roughness of the VIM molten Ti6Al4V sample was obtained with a Mitutoyo SJ-210 profilometer.

3. Results and Discussion

3.1. XRD analysis

X-ray diffraction spectra of commercial bar, chip and VIM molten Ti6Al4V is given in Figure 3 and Figure 4, respectively. The patterns presented for each sample are mostly consist from α (hexagonal close packed-hcp) phase.

XRD patterns of the chip and VIM molten Ti6Al4V show similar diffraction patterns. α and β (body centered cubic-bcc) phase peaks are different only as to intensity. The peak intensities of VIM molten Ti6Al4V are almost the same as commercial Ti6Al4V bar but slightly higher than the Ti6Al4V chip spectrum because of the finer structure in VIM molten Ti6Al4V.

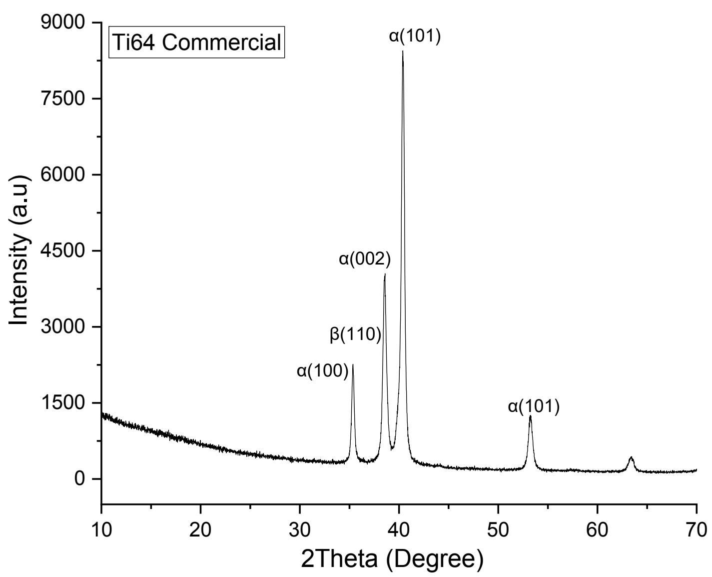

Figure 3. X-ray diffraction spectra of commercial Ti6Al4V bar

Between about 35° and 41°, the peaks occured for the planes (110) given by the body centered cubic structure, and also by planes (100), (002) and (101) of hexagonal close packed structure. The low intensity (110) peak indicates that a small amount of β phase is maintained in the final microstructure. Thereby, it is approved that the microstructure of VIM molten Ti6Al4V consists of α and β phases.

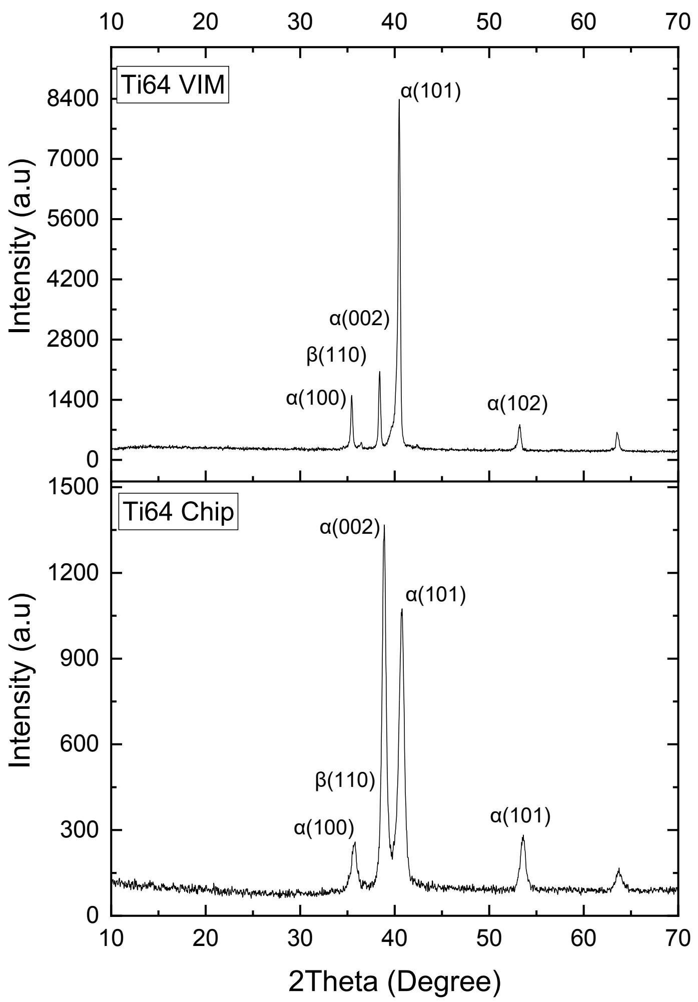

Figure 4. X-ray diffraction spectra of Ti6Al4V samples; chip and VIM molten

After melting, the crystallographic orientation of the VIM molten sample was re-organized and finally the crystal structure was formed that have the grains with (101) plane. The phase analysis results are consistent with the values presented in literature. According to Formanoir et al. (2016) and Balla et al. (2014) the final results support the microstructural changes related to phase transformation and indicate that VIM molten Ti6Al4V contain α (hcp) and β (bcc) phases after melting process. In addition, compared to chip and VIM molten Ti6Al4V, the peak intensities of α phases increased considerably after melting.

The crystal size of the samples was calculated using the Debye-Scherrer equation which is Equation (1) (Suryanarayana, 2001):

$$D=K\lambda/B\cos\Theta \qquad (1)$$

where K (0,9) is the numerical factor often called the crystallite-shape factor, D is the crystallite size, λ is the wavelength of the X-rays, B is the peak full width at half of the maximum intensity (FWHM) in radians, and Θ is the Bragg angle in radians. The crystal size of the samples is given in Table 1. According to this, the average crystal size of the commercial Ti6Al4V bar, chip and molten sample was calculated as about 18.5, 13.1 and 29.2 nm, respectively. It was found that the crystal size of the molten sample was larger than the crystal size of the commercial Ti6Al4V bar and chip.

Table 1. The crystallite size of the Ti6Al4V samples

Sample (Ti-6Al-4V)	Peak position (2Θ)	FWHM (B)	Crystallite size (D) (nm)	Average D (nm)
VIM molten	35.45	0.265	31.39	29.25
	38.40	0.258	32.56	
	40.46	0.315	26.86	
	53.20	0.350	25.37	
	63.56	0.310	30.08	
Chip	35.71	0.674	12.36	13.17
	38.88	0.565	14.88	
	40.71	0.753	11.24	
	53.57	0.652	13.63	
	63.72	0.680	13.73	
Commercial bar	35.35	0.332	25.05	18.51
	38.56	0.480	17.49	
	40.39	0.448	18.89	
	53.25	0.534	16.62	
	63.39	0.635	14.69	

3.2. Optical Microscopy analysis

Figure 5, which clearly shows fine needle-shaped structure with multi-directional distribution, represents the optical micrographs of VIM molten Ti6Al4V sample. The microstructure of VIM molten sample essentially consists of an α phase and a small amount of β within columnar grains.

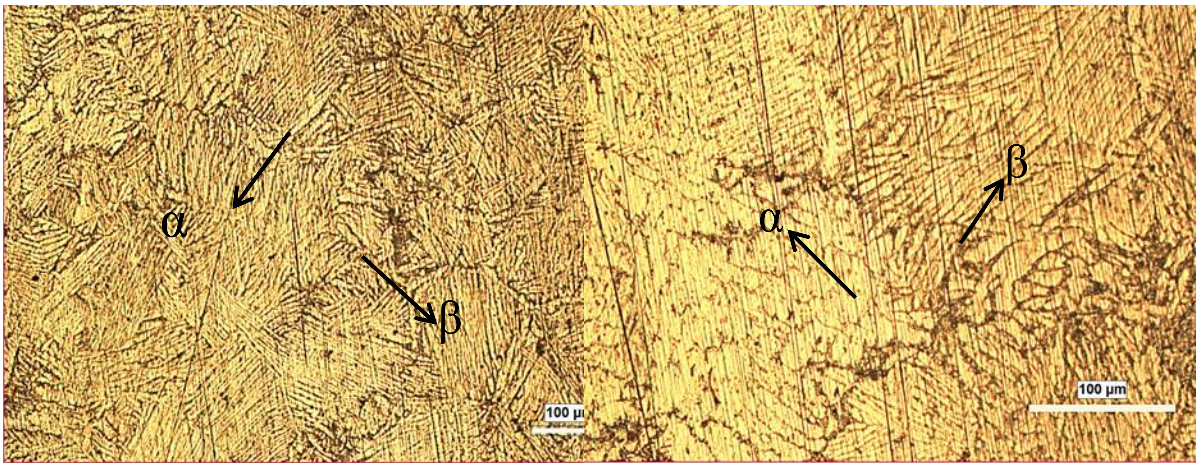

(a) 100X (b) 200X

Figure 5. Optical micrographs at different magnifications of VIM molten Ti6Al4V

The α phase possesses α lamellar morphology with β surrounding the α lamellar boundary. However, β columnar grain boundaries are obviously observed. α (hcp) phases are shown in bright surface and β (bcc) phases are seen in regions indicated by dark surface. The lamellar of the α phase (shown light) are relatively regular. The microstructure of VIM molten sample is lamellar due to resulting from rapid cooling from the high-temperature β phase. This was previously reported by Safdar et al. (2012) and Reginster et al. (2013).

A small pores were formed during melting as shown in Figure 6. The pores are mostly flat or irregular-shaped and formed at the interface between grain boundaries and the sizes of the pores range from 10 μm to 30 μm in diameter. The pores are caused by residual stresses due to increased temperature rapidly and rapid cooling afterwards and incomplete solidification (Qiu, & Attallah, 2013), (Vilaro et al., 2012), (Amato et al., 2012), (Thijs et al., 2010), (Facchini et al., 2010). The minimum porosity level that can be achieved in the molten sample is around 0.45%. The density of the molten sample was calculated as 4.41 g/cm^3. It is very close to the density of the commercial Ti6Al4V alloy (4.43 g/cm^3).

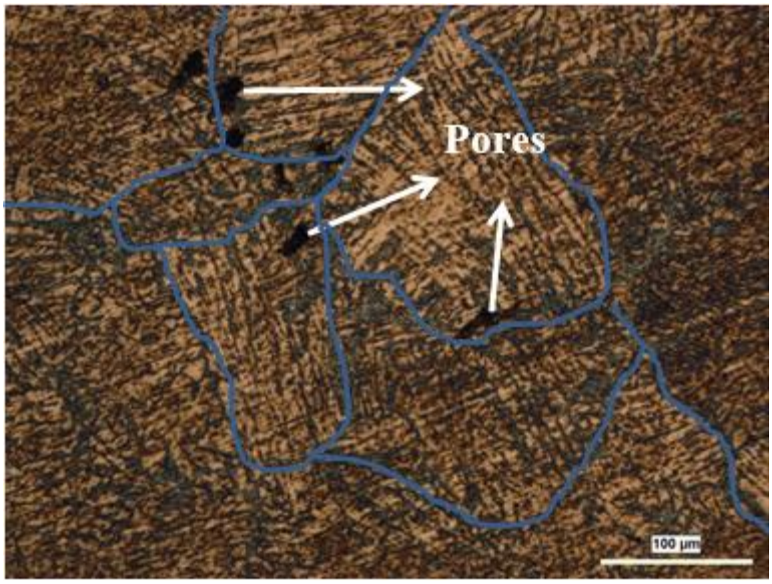

Figure 6. The pores in VIM molten Ti6Al4V sample

Moreover, surface roughness range of the VIM molten sample is very restricted after polished and the average roughness Ra 0.08 μm. The roughness measurement results show that a quite fine surface could be obtained by VIM.

3.3. SEM and EDS analysis

Figure 7 indicates SEM images taken from the rough and smooth sides of Ti6Al4V chip. During machining process of Ti6Al4V, the workpiece undergoes large deformation at high strain rate and temperature, which can change the microstructure and material properties of the Ti material and chip. Therefore, for surface characterization of Ti6Al4V chip, EDS was used to investigate the surface compositions after the cleaning process.

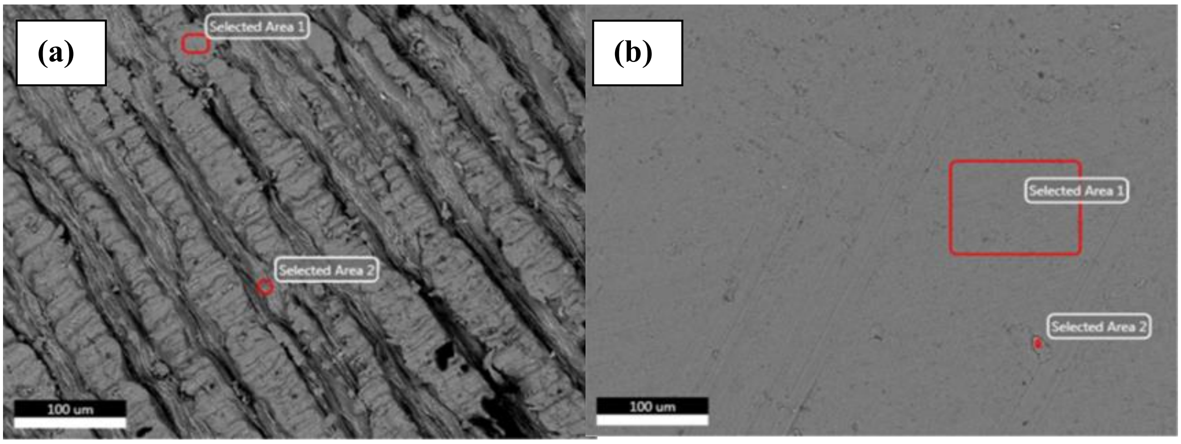

Figure 7. SEM images and EDS point analysis of Ti6Al4V chip at 500x magnification (a) rough side, (b) smooth side

The elemental distribution of the selected regions on the chip is given in Table 2. EDS analysis of both side of chip showed that oxygen (O) and carbon (C) ratios are high.

Table 2. Elemental composition of the Ti6Al4V chip

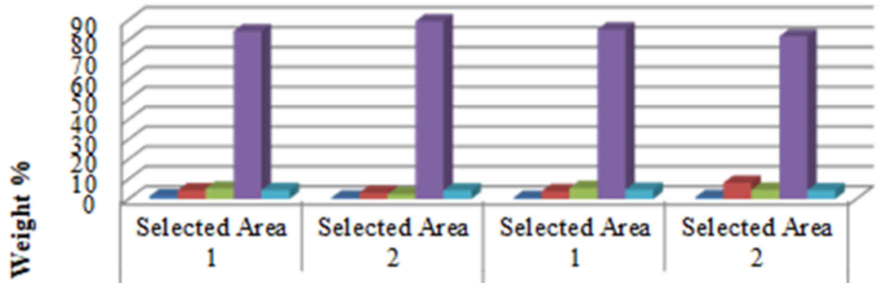

	Chip rough side		Chip smooth side	
	Selected Area 1	Selected Area 2	Selected Area 1	Selected Area 2
C	1.37	0.69	0.6	0.93
O	4.43	3.14	3.87	8.13
Al	5.26	2.43	5.55	4.65
Ti	84.42	89.38	85.29	81.81
V	4.53	4.36	4.69	4.47

The effect of machining atmosphere and temperature are considered as important reasons. Thus, the locate surface of impurity atoms such as O and C accelerate. Another factor can be interpreted as the fact that the waste chip can not be completely purified from the impurities as a result of the washing process. SEM images and selected areas for EDS analysis of molten Ti6Al4V sample is given in Figure 8.

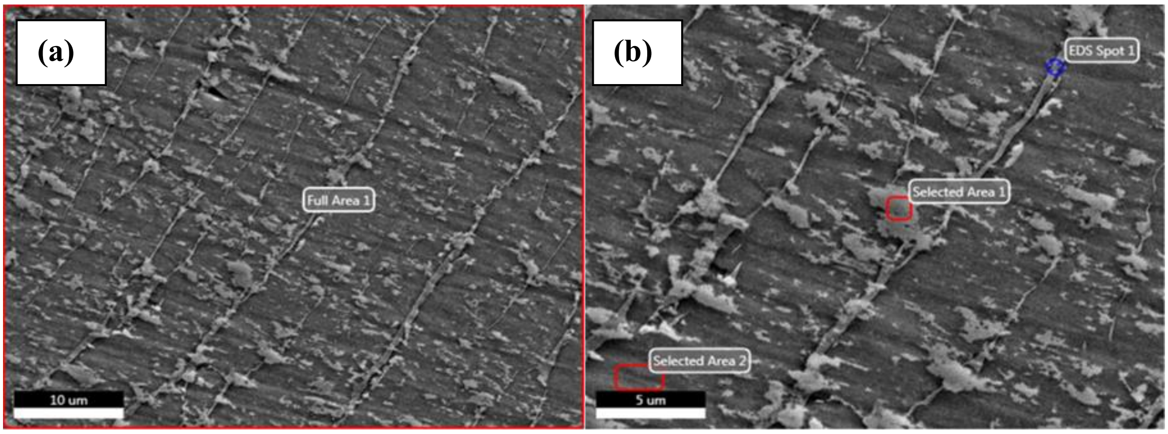

Figure 8. SEM images and EDS analysis of VIM molten Ti6Al4V sample at different magnifications of (a) 500X and (b) 2500X

The chemical composition of VIM molten Ti6Al4V was determined by EDS analysis, given in Table 3.

Table 3. Elemental distribution (EDS) of VIM molten Ti6Al4V sample

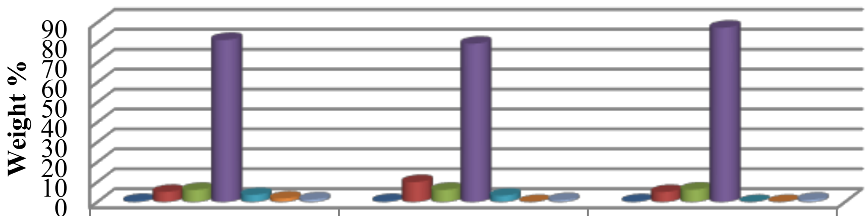

	Full Area	Selected Area 1	Selected Area 2
C	0.48	0.45	0.35
O	5.04	9.99	4.98
Al	6.04	6.08	6.19
Ti	81.29	79.39	87.41
V	3.59	3.2	0
N	1.72	0	0
Si	1.19	0.89	1.06

3.4. Hardness analysis

HRC hardness test was conducted on molten sample at room temperature. A total of five HRC hardness tests were conducted and their average was taken as the representative hardness value. The average Rockwell C Hardness (HRC) value of 51.4 was measured for the VIM molten sample. This result is quite high as compared to the work of Moon et al. [11]. Therefore, heat treatment is required after melting. Some researchers have already shown that the hardness of Ti and its alloys increases due to increased impurities such as O, C and N_2. N_2, O, and C reduce impact toughness of the material and increase the brittleness (Moon et al., 2017), (Oh, & Lim, 2016), (Su et al., 2009), (Vutova et al., 2010), (Roh et al., 2014), (Ahmet et al., 2017), (Sazak, 1999), (Rudnev et al., 2003), (Formanoir et al., 2016), (Balla et al., 2014),), (Suryanarayana, 2001), (Safdar et al., 2012), (Reginster et al., 2013), (Qiu, & Attallah, 2013), (Vilaro et al., 2012), (Amato et al., 2012), (Thijs et al., 2010), (Facchini et al., 2010), (Wasz et al., 1996). It was shown by EDS that C, O and N_2 ratios are above limits.

4. Results and Discussions

With the increased awareness of the circular economy, the recovery of precious materials is of great importance for the materials world and the environment. In this study, we have carried out an important study to convert the waste titanium scrap into molten titanium. It has been clearly shown that scrap titanium obtained from implant industry can be melted and cast titanium alloy has been obtained. Detailed analysis showed that we could obtain high purity titanium alloy with the scrap. We believe that the technique developed here will help the researchers to find new ways to recycle the metallic materials and this will open many fruitful papers in the scientific community and for the industrial applications. For future studies, advanced chip cleaning and purification should be carried to obtain higher quality melted products.

Acknowledgements

The authors would like to thank Metrosan Medical Company (Manisa, Turkey) for providing the raw materials and Ervak Makine Company for using VIM machine. Thanks are also Birim Makina Company for their support to the compressed into a cylindrical briquette.

Author Statement

Erdoğan Teke: Conception and design of study, Methodology, Writing- Original draft preparation. Mücahit Sütçü: Data curation, Writing- Original draft preparation. Yıldıray Başkurt: Conception and design of study, Investigation. M. Özgür Seydibeyoğlu: Supervision, Writing- Reviewing and Editing.

Conflict of Interest

The authors declare no conflict of interest.

References

Ahmed, N., Abdo, B.M., Darwish, S., Moiduddin, K., Pervaiz, S., Alahmari, A.M., & Naveed, M. (2017). Electron beam melting of titanium alloy and surface finish improvement through rotary ultrasonic machining, *The International Journal of Advanced Manufacturing Technology*, 92, 3349–3361.

Amato, K.N., Gaytan, S.M., Murr, L.E., Martinez, E., Shindo, P.W., Hernandez, J., Collins, J., & Medina, F. (2012). Microstructures and mechanical behavior of Inconel 718 fabricated by selective laser melting, *Acta Materialia*, 60, 2229–2239.

ASM Handbook, (2008). Casting, Volume 15, USA, ASM International.

Balla, V.K., Soderlind, J., Bose, S., & Bandyopadhyay, A. (2014). Microstructure, mechanical and wear properties of laser surface melted Ti6Al4V alloy, *Journal of*

Mechanical Behavior of Biomedical Materials, 32, 335-344.

Destefani, J.D. (1990). *Introduction to Titanium and Titanium Alloys. Properties and selection: Nonferrous alloys and special-purpose materials*, Volume 2, ASM International, Ohio, 586-591.

Dikici, T., & Sutcu, M. (2017). Effects of disc milling parameters on the physical properties and microstructural characteristics of Ti6Al4V powders, *Journal of Alloys and Compounds*, 723, 395-400.

Donachie Jr., M.J. (2000). *Titanium: A Technical Guide*, ASM International, USA.

Facchini, L., Magalini, E., Robotti, P., & Molinari, A. (2009). Microstructure and mechanical properties of Ti-6Al-4V produced by electron beam melting of pre-alloyed powders, *Rapid Prototyping Journal*, 15(3), 171-178.

Facchini, L., Magalini, E., Robotti, P., Molinari, A., Hoges, S., & Wissenbach, K. (2010). Ductility of a Ti-6Al-4V alloy produced by selective laser melting of prealloyed powders, *Rapid Prototyping Journal*, 16, 450–459.

Formanoir, C., Michotte, S., Rigo, O., Germain, L., & Godet, S. (2016). Electron beam melted Ti–6Al–4V: Microstructure, texture and mechanical behavior of the as-built and heat-treated material, *Materials Science & Engineering A*, 652, 105–119.

Froes, F.H. (2013). *Powder Metallurgy of Titanium Alloys. Advances in Powder Metallurgy*, Woodhead Publishing, Cambridge, 202-240.

Leyens, C. & Peters, M. (2003). *Titanium and Titanium Alloys: Fundamentals and Applications*. Wiley-Vch, Weinheim.

Moon, B., Seo, J. H., Lee, H., Jung, K. H., Park, J. H., & Jung, H. (2017). Method of recycling titanium scraps via the electromagnetic cold crucible technique coupled with calcium treatment, *Journal of Alloys and Compounds*, 727, 931-939.

Neff, D.V. (1990). Recycling of Nonferrous Alloys, in: *ASM Handbook Committee (Eds.), Properties and selection: Nonferrous alloys and special-purpose materials*, volume 2, ASM International, Ohio, 1205-1232.

Oh, J., Roh, K., & Lim, J. (2016). Brief review of removal effect of hydrogen-plasma arc melting on refining of pure titanium and titanium alloys, *International Journal of Hydrogen Energy*, 41, 23033 – 23041.

Qiu, C., Adkins, N., & Attallah, M. (2013). Microstructure and tensile properties of selectively laser-melted and of HIPed laser-melted Ti–6Al–4V, *Materials Science and Engineering: A*, 578(20), 230–239.

Rack, H.J., & Qazi, J.I. (2006). Titanium alloys for biomedical application, *Materials Science and Engineering: C*, 26(8), 1269-1277.

Reginster, S. et al., (2013). Processing of Ti alloys by additive manufacturing: a comparison of the microstructures obtained by laser cladding, selective laser melting and electron beam melting, *Materials Science Forum*, 765, 413–417.

Roh, K., Suh, C., Oh, J., Kim, W., Kwon, H., & Lim, J. (2014). Comparison of deoxidation capability for preparation of low oxygen content powder from TiNi alloy scraps, *Powder Technology*, 253, 266–269.

Rudnev, V., Loveless, D., Cook, R., & Black, M. (2003). *Handbook of Induction Heating*, Marcell Dekker Inc., New York.

Safdar, A. et al., (2012). Evaluation of microstructural development in electron beam melted Ti–6Al–4V, *Materials Characterization*, 65, 8–15.

Sazak, B.S. (1999). Design of a 500W Resonant Induction Heater, *Pamukkale University Journal of Engineering Sciences*, 5(1), 871-878.

Su, Y., Wang, L., Luo, L., Jiang, X., Guo, J., & Fu, H. (2009). Deoxidation of Titanium alloy using hydrogen, *International Journal of Hydrogen Energy*, 34, 8958 – 8963.

Suryanarayana, C. (2001). Mechanical alloying and milling, *Progress in Materials Science*, 46, 1-184.

Thijs, L., Verhaeghe, L., Craeghs, T., Humbeeck, J.V., Kruth, J.P. (2010). A study of the microstructural evolution during selective laser melting of Ti-6Al-4V, *Acta Materialia*, 58, 3303–3312.

Topolski, S., Bochniak, W., Lagoda, M., Ostachowski, P., & Garbacz, H. (2017). Structure and properties of titanium produced by a new method of chip recycling, *Journal of Materials Processing Technology*, 248, 80–91.

Vilaro, T., Colin, C., Bartout, J.D., Naze, L., & Sennour, M. (2012). Microstructural and mechanical approaches of the selective laser melting process applied to a nickel-base superalloy, *Materials Science and Engineering: A*, 534, 446–451.

Vutova, K., Vassileva, V., Koleva, E., Georgieva, E., Mladenov, G., Mollov, D., & Kardjiev, M. (2010). Investigation of electron beam melting and refining of titanium and tantalum scrap, *Journal of Materials Processing Tech*nology, 210(8), 1089–1094.

Wasz, M., Brotzen, F., McLellan, R., & Griffin, A. (1996). Effect of oxygen and hydrogen on mechanical properties of commercial purity titanium, *International Materials Reviews*, 41(1), 1-12.

Scientific Research Communications
Research Article
Sci. Res. Comm. (2022)
Volume 2, Issue 1
doi: 10.52460/src.2022.002

Manufacturing and Modeling of Polypropylene-based Hybrid Composites by Using Multiple-Nonlinear Regression Analysis

Melih Savran[1], Muhammed Yılmaz[2], Mustafa Öncül[1], Kutlay Sever[1,*]

[1] Department of Mechanical Engineering, İzmir Kâtip Çelebi University, Turkey
[2] Plato Vocational School, Department of Motor Vehicles and Transportation Technologies, İstanbul Ayvansaray University, İstanbul, Turkey
**Corresponding author: kutlay.sever@ikcu.edu.tr*

Received: 04.11.2022 Accepted: 22.01.2022

Abstract

In this research, artichoke stem particles and wollastonite were used as organic and inorganic fillers in order to improve the mechanical properties of polypropylene. In this regard, PP-matrix composites containing AS and W were produced as non-hybrid and hybrid using a high-speed thermo-kinetic mixer. Mechanical properties of polymer composites were investigated by the tensile test. Experimental results reveal that the highest elastic modulus was obtained in PP-W, and the highest tensile strength was obtained in raw PP while the lowest ultimate strain value was obtained in PP-W-AS. Then, multiple-nonlinear regression analysis was employed to determine the effect of weight ratios of W and AS in PP on elastic modulus, tensile strength, and ultimate strain. Experimental results were expressed with polynomial, rational, and trigonometric models. The results show that the proposed models fit well with the experimental results. The coefficient of determination (R^2) values were found between 0.95 and 1 in all models. Also, boundedness check control of the proposed models, which gives information about whether models are realistic or not, was carried out by calculating the maximum and minimum values produced by the relevant model.

Keywords: hybrid polymer composites, multiple-nonlinear regression, boundedness check, modeling

1. Introduction

In recent decades, synthetic fibers have been replaced by lignocellulosic fibers in many industrial and daily applications. Automotive interior parts and non-structural building applications that do not require high strength and high thermal stability come to the forefront among these application areas. Researchers working on the development of polymer matrix composite materials demand to design and manufacture recyclable materials in order to minimize the effects of damage to the environment. In the production of thermoplastic matrix composite materials, lignocellulose based fibers such as kenaf, cotton, sisal, jute, ramie, sugar cane, coconut fiber are used together with thermoplastics in order to reduce the production cost and to minimize the damage to the environment (Rong et al., 2001; Saba et al., 2015; Sever et al., 2012; Verma & Gope, 2015; Xu et al., 2010). In addition, agricultural wastes such as vine stem, olive pomace, corn, wheat, rice, almond shell, and lignocellulose-rich corn cob were used as filling/reinforcement material (Essabir et al., 2013; Guimarães et al., 2009; Kaya et al., 2018; Kılınc et al., 2016; Mengeloglu & Karakus, 2008; Nourbakhsh & Ashori, 2010; Yao et al., 2008). Although such non-hybrid studies are widespread in the literature, the number of studies on agricultural waste and mineral-filled hybrid composites is limited. The use of hybrid structures aims to provide many essential features in engineering design, such as reducing material weight, increasing strength, reducing production costs, improving thermal properties, and ensuring easy recycling of materials (Mattos et al., 2014).

In the manufacturing of composites, lignocellulosic materials are used as filling/reinforcement materials, and thermoplastics such as polypropylene (PP), polyethylene (PE) and polylactic acid (PLA) are used as matrix materials. In scientific studies, it has been observed that the use of lignocellulosic materials using as filler/reinforcement with different matrix materials in the production of composites has increased significantly. Thermoplastic matrix material PP is one of the most important commercial polyolefins, and it has a wide range of uses from the automotive and aerospace industries to household plastic products. Various filling materials can be added to the matrix to provide the desired physical and mechanical properties and low cost. Lignocellulosic fillers and mineral fillers can be mixed into the thermoplastic polymer matrix as a hybrid form and can directly affect the composite materials' physical, mechanical, and thermal properties. Although the experiment is an important process to determine mechanical and physical properties of lignocellulose-based hybrid composites, it is worth noting that putting forward mathematical models that can correctly explain and verify the experimental results is a necessity that cannot be ignored. In this regard, Response Surface Method and ANOVA are frequently used together in the literature (Ashenai Ghasemi et al., 2016; Ayaz et al., 2018; Nor et al., 2021; Ragunath et al., 2021; Srivabut et al., 2021; Syed et al., 2020; Yiga et al., 2021). Supporting the experimental results with mathematical models makes it possible to create alternative designs, determine the effects of the design parameters correctly, and depending on these can be improved the obtained values of the response variables. In this respect, Syed et al. (2020) considered optimization of talc filled polypropylene material. In the study, a Taguchi-based multi-objective approach was used to maximize tensile strength and minimize shrinkage simultaneously. It was seen that selected as design parameters: injection pressure, injection speed, mold temperature, and melt temperature had a significant effect on tensile strength and shrinkage. As a result of the optimization process, the tensile strength was found as 24.40 MPa with 10% increment, and the shrinkage was found as 2.28% with a 30% reduction. Ghasemi et al. (2016) optimized tensile strength, tensile modulus, and impact resistance of polypropylene-based hybrid composites. In order to examine the effects of three design parameters loading ratios of talc, maleic anhydride grafted polypropylene (MAPP), and talc and exfoliated graphene nanoplatelets (xGnPs) fillers on mechanical properties, fifteen experiments were designed utilizing Box Behnken method. Researchers proposed second-order polynomial models with response surface methodology to determine the effects of design parameters on mechanical properties. It was shown that the talc and xGnP fillers ratios considerably affect the mechanical properties. They found that the desirable values of the design parameters to maximize mechanical properties simultaneously were 30 wt% for talc, 4 wt% for MAPP, and 0.69 wt% for xGnP. Yiga et al. (2021) conducted a study to enhance the tensile strength of fiber-reinforced PLA composites. Rice husk fiber and clay filler were employed as additive materials. The effects of five design factors, clay filler loading, rice husk variety, rice husk fiber loading, alkali type, and alkali concentration on tensile strength, were determined by variance analysis (ANOVA). Filler loading and fiber loading factors were found as the most significant model terms. In another study in which the response surface method came to the fore, the mechanical and physical properties of wood-plastic composites were mathematically modeled using linear and quadratic functions. The coefficient of determination (R^2) parameter was considered as a success criterion to evaluate the prediction performance of proposed models. It was found that the R^2 gets changing values between 0.86 and 0.99 for all models (Srivabut et al., 2021). The experimental investigation and mathematical modeling were carried out regarding the mechanical properties of sisal and glass fiber reinforced hybrid composite (Ragunath et al., 2021). Tensile and flexural strength results of material were modeled with second-order polynomial while impact strength results were predicted well fit by a linear model. Sisal and epoxy volume fraction was considered as design variables, and the effects of those parameters on mechanical properties were investigated. It was understood that while the sisal has the more important effect on tensile and impact strength results of hybrid composite, it hasn't a noticeable effect on flexural strength results. In the literature, it is seen that there are many studies regarding design, modeling, and optimization to improve the mechanical properties of recyclable hybrid composites. However, to evaluate the success of the models proposed in these studies, criteria such as R^2, R^2 adjusted, and R^2 predicted, which show the relationship between observed and predicted values, are taken into consideration. These criteria alone may not be sufficient to test the success of a model. In this context, Polatoğlu et al. (2020) came up with boundedness check as an additional success criterion to evaluate whether the proposed mathematical model is appropriate or not.

The present paper examined the production of AS and W-filled PP hybrid and non-hybrid composite materials. The elastic modulus, ultimate tensile strength, and strain of the composite materials were obtained by experimentally. Multiple-nonlinear regression analysis was used in the modeling of the experimental results. In this regard, polynomial, rational, trigonometric models and their performance in estimating observed values were compared with each other. It was shown that the R^2 success criterion was insufficient to describe experimental results accurately. As an additional criterion, the importance of boundedness check in model selection was emphasized.

2. Materials and Methods

In this work, lignocellulose-based artichoke stem particles (AS), mineral-based wollastonite (W), and AS-W as hybrid were used to improve the mechanical properties of polypropylene (Table 1). The PP-copolymer (PP, LG Chem M 1500, Korea) used in this study has a melt flow index of 16 g/10 min. (230 °C/2.16 kg) and a density of 0.9 g/cm^3. Artichoke stems were supplied from the products left as agricultural waste from an artichoke fruit plant field in Çiğli, İzmir. To make artichoke stems suitable for milling, stems were broken into small pieces then mill with a laboratory-type grinder. Later on, artichoke stem particles were passed through 60 and 140 mesh sieves (Retsch RS200, Germany). Particle sizes in the range of 100 μm-250 μm were used to produce composites. Wollastonite (Tremin 939-300 needle-shaped, untreated, density=2.85 g/cm^3 and Mohs hardness=4.5) was obtained from Kaolin Industrial Minerals, İstanbul.

The production of hybrid and non-hybrid polymer composites was carried out to a laboratory-scale high-speed thermo-kinetic mixer and a laboratory-type heated-cooled hydraulic press (Gülnar Makina, Turkey). The mechanical properties (ultimate tensile strength, ultimate strain, and elastic modulus) of these materials were obtained using a tensile testing machine (Shimadzu AGS-X, 5 kN, Japan). Tests were carried out according to "ASTM D638-14 Standard Test Method for Tensile Properties of Plastics" (D20 Committee, n.d.). The cross-head speed was determined as 50 mm/min during the tensile test. The tests were repeated at least five times for each type of material produced to increase the sensitivity of the tests. Test results were determined according to the average values, taking into account the standard deviations. Table 1 shows the mixing ratios of the materials. The results signed with a star in Table 1 are taken from the literature (Sever & Yılmaz, 2020).

Table 1. The mixing ratios of the materials

Trial	Material	Wollastonite (wt %)	Artichoke stem (wt %)
1	PP*	0	0
2	PP-10AS*	0	10
3	PP-20AS*	0	20
4	PP-30AS*	0	30
5	PP-10W	10	0
6	PP-20W	20	0
7	PP-30W	30	0
8	PP-3W-7AS*	3	7
9	PP-7W-3AS*	7	3
10	PP-5W-5AS*	5	5
11	PP-10W-10AS	10	10
12	PP-14W-6AS	14	16
13	PP-6W-14AS	6	14
14	PP-15W-15AS	15	15
15	PP-21W-9AS	21	9
16	PP-9W-21AS	9	21

3. Regression Analysis

The researchers try to find the most appropriate models which correctly estimate the results obtained using experimental or numerical methods. Regression analysis is one of the statistical methods used for this purpose. There are distinct type of mathematical models to estimate relationship between independent and dependent parameters. Among these, models including only linear functional terms are appropriate for problems whose non-complex and having few independent variables. In case the relationship between parameters is nonlinear, a regression model consisting of advanced mathematical functions would be more suitable to many engineering processes (Aktaş

& Aydın, 2021). In the literature, the most commonly used criteria for evaluating model success is coefficient of determination. R^2 consists of two parameters that show the relationship between predicted-observed and observed-mean values and are named as the sum of square error and the total sum of square, respectively (Equation 1). The fact that the R^2 value is close to 1 indicates that the proposed mathematical model very well defines the phenomena.

$$SSE = \sum_{i=1}^{n}(x_i - \hat{x}_i)^2 \qquad SST = \sum_{i=1}^{n}(x_i - x_{mean})^2 \qquad R^2 = 1 - \frac{SSE}{SST} \tag{1}$$

where $x_i, , x_{mean,}\ \hat{x}_i\ and$ n show observed, mean, predicted values and the number of rows, respectively.

4. Results and Discussions

In this section, various regression models have been proposed for PP-based hybrid materials design. In the modeling phase, experimental data were produced within the scope of this study, and some (signed with star in Table 1) were obtained from the study conducted by Sever and Yılmaz (2020) were used. Considered PP-based hybrid composite includes artichoke stem and wollastonite as filler. First, the effect of the weight ratio of AS and W fillers regarding elastic modulus, ultimate tensile strength, and ultimate strain is investigated experimentally. After that, 12 distinct regression models with two parameters were tested in terms of fitting performance.

Figure 1 shows experimental results regarding the mechanical properties of PP-based non-hybrid and hybrid materials with different weight ratios of AS, W, and AS-W fillers. It is seen that the hybridization process negatively affected the strength performance of the PP material, where raw PP material gives the best results (22.34 MPa) in terms of ultimate strength. When the elastic modulus and strain results are evaluated, it can be said that while filling of PP with 30% W (PP-30W) provides the highest elastic modulus, hybridization of PP with 15% W and 15% AS (PP-15W-15AS) gives the lowest strain value.

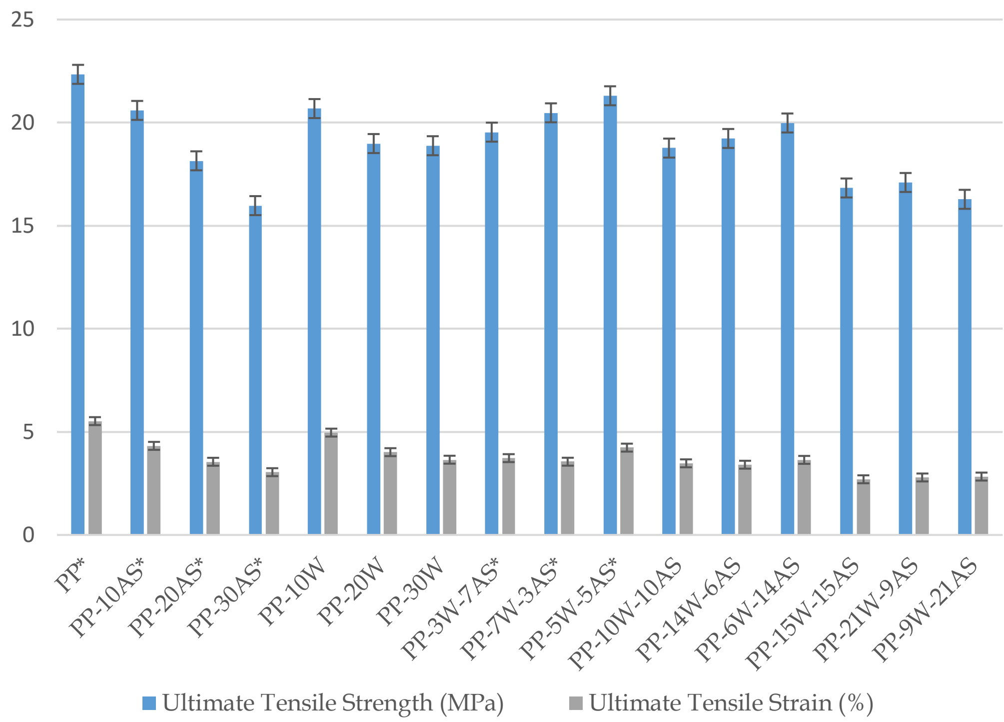

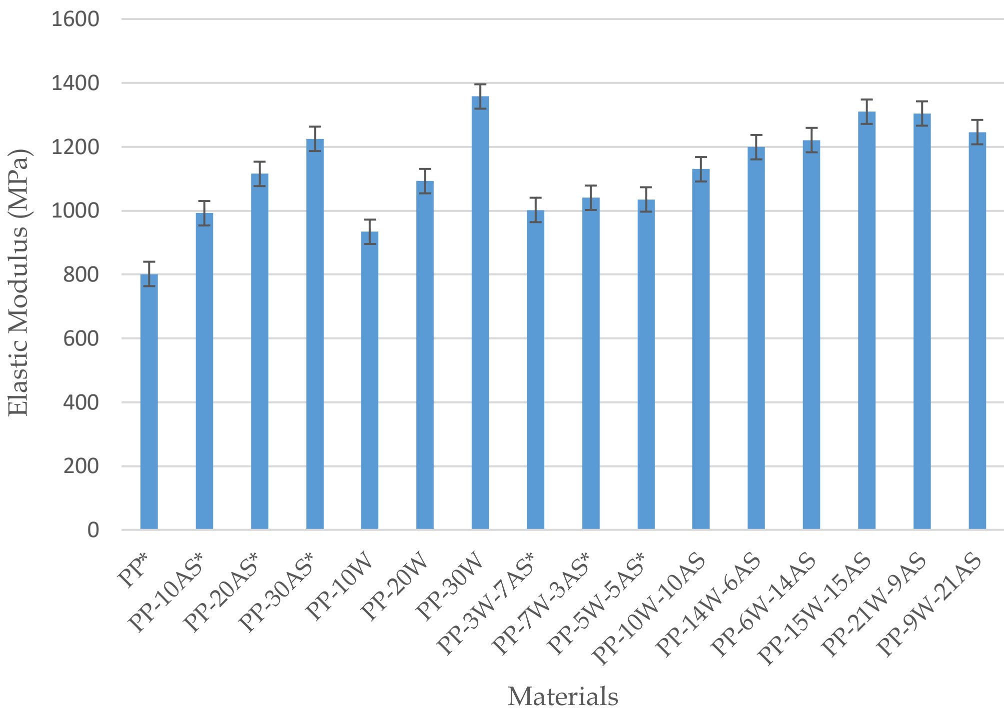

Figure 1. Mechanical properties of PP-based composite materials

In the modeling phase, multiple nonlinear regression analysis was used to describe phenomena mathematically regarding elastic behavior of PP-based hybrid composites given in Figure 1. Proposed four distinct models and their fitting performance was given in Tables 2 and 3.

Table 2. Multiple nonlinear mathematical models for elastic modulus

Name	Models
Third order multiple nonlinear (TON)	$Y = 801.6 + 24.73x_1 - 0.6392x_1^2 + 0.009467x_1^3 + 22.17x_2 + 1.198x_1x_2 - 0.04765x_1^2x_2 - 0.9281x_2^2 - 0.02881x_1x_2^2 + 0.02688x_2^3$
Fifth order multiple nonlinear (FION)	$Y = 801.6 + 23.04x_1 - 0.7127x_1^2 + 0.05279x_1^3 - 0.002737x_1^4 + 0.00004797x_1^5 + 16.36x_2 + 4.502x_1x_2 - 1.326x_1^2x_2 + 0.1346x_1^3x_2 - 0.003301x_1^4x_2 - 0.361x_2^2 + 0.8592x_1x_2^2 - 0.1052x_1^2x_2^2 + 0.0008965x_1^3x_2^2 - 0.01527x_2^3 - 0.04608x_1x_2^3 + 0.00385x_1^2x_2^3 + 0.002335x_2^4 + 0.0004718x_1x_2^4 - 0.00004482x_2^5$
Third order multiple nonlinear rational (TONR)	$Y = (17.83 + 783.4x_1 + 10036.x_1^2 - 196.1x_1^3 - 1283.x_2 - 14918.x_1x_2 + 171.3x_1^2x_2 - 1553.x_2^2 + 63.24x_1x_2^2 + 159.1x_2^3)/(0.02224 + 17.87x_1 + 8.242x_1^2 - 0.1809x_1^3 - 18.64x_2 - 15.91x_1x_2 + 0.2274x_1^2x_2 + 1.17x_2^2 + 0.1519x_1x_2^2 + 0.05974x_2^3)$
Third order trigonometric multiple nonlinear (TOTN)	$279.3 + 8.723\mathrm{Cos}(x_1) + 298.9\mathrm{Cos}(x_1)^2 - 2.066\mathrm{Cos}(x_1)^3 + 13.81\mathrm{Cos}(x_2) + 122.1\mathrm{Cos}(x_1)\mathrm{Cos}(x_2) - 88.45\mathrm{Cos}(x_1)^2\mathrm{Cos}(x_2) + 273.8\mathrm{Cos}(x_2)^2 - 111.2\mathrm{Cos}(x_1)\mathrm{Cos}(x_2)^2 + 6.739\mathrm{Cos}(x_2)^3 + 29.41\mathrm{Sin}(x_1) + 169.9\mathrm{Cos}(x_1)\mathrm{Sin}(x_1) - 78.91\mathrm{Cos}(x_1)^2\mathrm{Sin}(x_1) - 187.3\mathrm{Cos}(x_2)\mathrm{Sin}(x_1) - 49.58\mathrm{Cos}(x_1)\mathrm{Cos}(x_2)\mathrm{Sin}(x_1) + 26.5\mathrm{Cos}(x_2)^2\mathrm{Sin}(x_1) + 441.3\mathrm{Sin}(x_1)^2 + 138.2\mathrm{Cos}(x_1)\mathrm{Sin}(x_1)^2 + 145.\mathrm{Cos}(x_2)\mathrm{Sin}(x_1)^2 + 65.66\mathrm{Sin}(x_1)^3 + 24.02\mathrm{Sin}(x_2) - 218.3\mathrm{Cos}(x_1)\mathrm{Sin}(x_2) + 25.03\mathrm{Cos}(x_1)^2\mathrm{Sin}(x_2) + 76.52\mathrm{Cos}(x_2)\mathrm{Sin}(x_2) - 59.11\mathrm{Cos}(x_1)\mathrm{Cos}(x_2)\mathrm{Sin}(x_2) - 65.56\mathrm{Cos}(x_2)^2\mathrm{Sin}(x_2) + 72.17\mathrm{Sin}(x_1)\mathrm{Sin}(x_2) - 355.3\mathrm{Cos}(x_1)\mathrm{Sin}(x_1)\mathrm{Sin}(x_2) - 322.2\mathrm{Cos}(x_2)\mathrm{Sin}(x_1)\mathrm{Sin}(x_2) + 40.49\mathrm{Sin}(x_1)^2\mathrm{Sin}(x_2) + 487.3\mathrm{Sin}(x_2)^2 + 157.6\mathrm{Cos}(x_1)\mathrm{Sin}(x_2)^2 + 117.8\mathrm{Cos}(x_2)\mathrm{Sin}(x_2)^2 + 65.69\mathrm{Sin}(x_1)\mathrm{Sin}(x_2)^2 + 53.88\mathrm{Sin}(x_2)^3$

Table 3 denotes the fitting and boundedness performance of mathematical models used to estimate the elastic behavior of PP-based hybrid composites. The most crucial parameter showing the usability of a mathematical model in the literature is the value of R^2. When the results are examined, it will be seen that except that "TON" R^2 values of all models are 1. If we made a model selection considering only the R^2 value, we could think that all the models explain the process well. However, R^2 alone does not correctly define the phenomena of the process. Further, boundedness check control of the proposed models, which gives information about whether models are realistic or not should be carried out. We can see if there is a functional limitation (bounded) by calculating the maximum and minimum values produced by the relevant model.

Table 3. Fitting performance and boundedness of models for elastic modulus

Model	R^2	Max.	Min.
TON	0.97	1357.23	801.6
FION	1	1399.29	801.6
TONR	1	2194.14	-31020
TOTN	1	1653.29	377.42

In this context, it has been accepted that the results of polynomial models "FION" and "TON" are suitable for the nature of the problem by expert researchers in production and material selection. However, the view that models "TONR" and "TOTN" give results that cannot be obtained experimentally came to the fore.

Figure 2 represents the 3D plot of polynomial, rational and trigonometric models that best fit the experimental results. When the graphics are examined, it is seen that the models accurately predict all the experimental data. However, as stated when evaluating the results of Table 3, a high R^2 value does not always give accurate information about the usability of the proposed model. Whether the mathematical model gives correct information should be checked with criteria other than R^2. In problems where the number of design variables is one or two, an evaluation can be made by graphically examining the model's results. Since the weight ratios of artichoke stem particles and wollastonite filler are selected as two design variables in this study, it is possible to evaluate the mathematical models graphically. Here, rational and trigonometric models ("TONR" and "TOTN") have many local maximum and minimum points, which insignificant changes in design parameters lead to a non-negligible difference in results. On the contrary, polynomial models ("FION" and "TON") show a stable and consistent distribution within the specified range of design parameters. Therefore, these models are appropriate to estimate mathematical phenomena regarding the elastic modulus of PP-based hybrid composite.

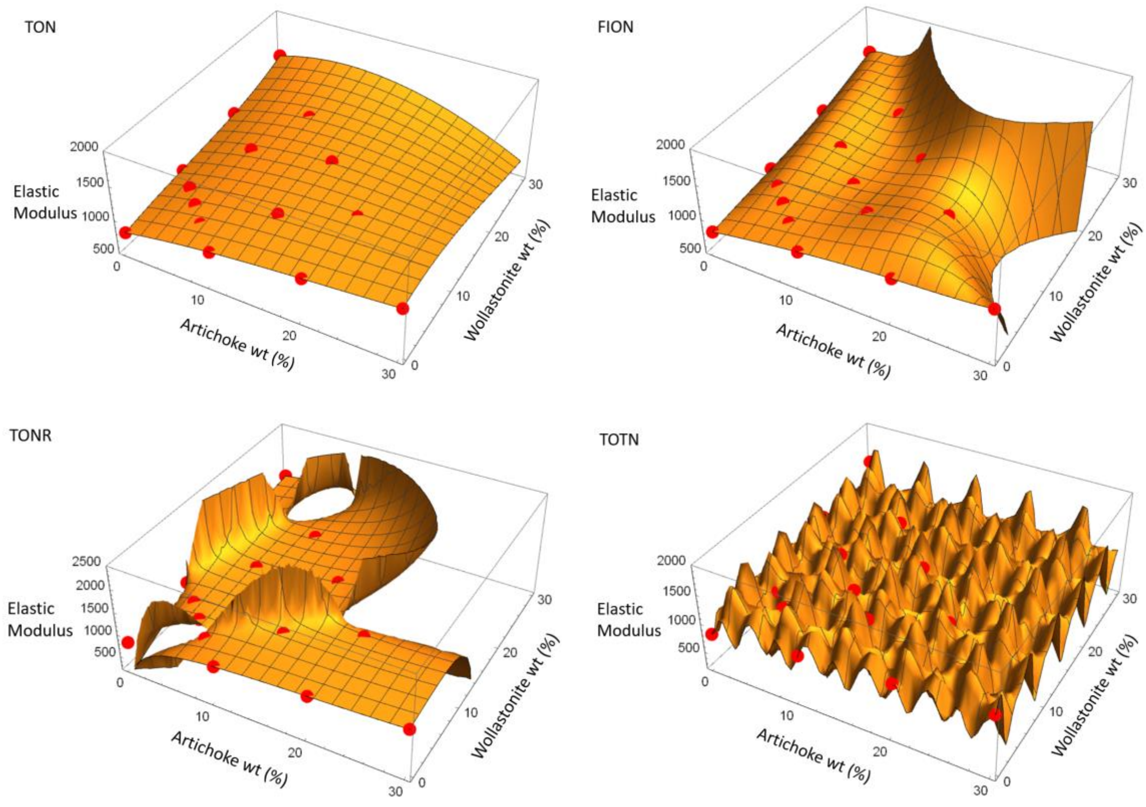

Figure 2. 3D plot representations of experimental data and recommended mathematical model for elastic modulus

Another mechanical parameter modeling with regression analysis was ultimate tensile strength. Four distinct mathematical models and their fitting performance were given in Tables 4 and 5.

Table 4. Mathematical models for ultimate tensile strength

Name	Models
Third order multiple nonlinear (TON)	$Y = 22.34 - 0.2984x_1 + 0.01022x_1^2 - 0.0002481x_1^3 - 0.1546x_2 + 0.02779x_1x_2 - 0.001013x_1^2x_2 - 0.004468x_2^2 - 0.0008286x_1x_2^2 + 0.0001926x_2^3$
Sixth order multiple nonlinear (SON)	$Y = 22.34 - 0.1237x_1 - 0.01134x_1^2 + 0.00002776x_1^3 + 0.0001375x_1^4 - (9.586 \times 10^{-6})x_1^5 + (1.76 \times 10^{-7})x_1^6 - 0.09966x_2 + 0.02216x_1x_2 - 0.01042x_1^2x_2 - 0.01065x_1^3x_2 + 0.0009603x_1^4x_2 - 0.00002011x_1^5x_2 - 0.008408x_2^2 + 0.01434x_1x_2^2 + 0.0215x_1^2x_2^2 - 0.0009108x_1^3x_2^2 - (1.304 \times 10^{-7})x_1^4x_2^2 - 0.0007965x_2^3 - 0.01181x_1x_2^3 - 0.0009454x_1^2x_2^3 + 0.00003689x_1^3x_2^3 + 0.0001704x_2^4 + 0.000916x_1x_2^4 + (2.702 \times 10^{-6})x_1^2x_2^4 - (8.699 \times 10^{-6})x_2^5 - 0.00001807x_1x_2^5 + (1.399 \times 10^{-7})x_2^6$
Second order multiple nonlinear rational (SONR)	$Y = (3141.8 - 51.011x_1 - 0.94323x_1^2 - 118.64x_2 - 2.0546x_1x_2 + 0.1594x_2^2)/(140.62 - 0.81531x_1 - 0.076061x_1^2 - 4.1694x_2 - 0.19421x_1x_2 - 0.033376x_2^2)$
Third order trigonometric multiple nonlinear (TOTN)	$Y = 4.622 + 0.7108\mathrm{Cos}(x_1) + 6.661\mathrm{Cos}(x_1)^2 + 1.155\mathrm{Cos}(x_1)^3 + 0.7972\mathrm{Cos}(x_2) - 1.973\mathrm{Cos}(x_1)\mathrm{Cos}(x_2) + 1.73\mathrm{Cos}(x_1)^2\mathrm{Cos}(x_2) + 6.162\mathrm{Cos}(x_2)^2 + 1.341\mathrm{Cos}(x_1)\mathrm{Cos}(x_2)^2 + 1.134\mathrm{Cos}(x_2)^3 + 0.2348\mathrm{Sin}(x_1) + 2.5\mathrm{Cos}(x_1)\mathrm{Sin}(x_1) - 1.035\mathrm{Cos}(x_1)^2\mathrm{Sin}(x_1) - 1.444\mathrm{Cos}(x_2)\mathrm{Sin}(x_1) - 1.021\mathrm{Cos}(x_1)\mathrm{Cos}(x_2)\mathrm{Sin}(x_1) + 1.34\mathrm{Cos}(x_2)^2\mathrm{Sin}(x_1) + 4.167\mathrm{Sin}(x_1)^2 - 2.086\mathrm{Cos}(x_1)\mathrm{Sin}(x_1)^2 + 0.2159\mathrm{Cos}(x_2)\mathrm{Sin}(x_1)^2 + 0.6172\mathrm{Sin}(x_1)^3 + 0.001065\mathrm{Sin}(x_2) - 2.13\mathrm{Cos}(x_1)\mathrm{Sin}(x_2) + 1.414\mathrm{Cos}(x_1)^2\mathrm{Sin}(x_2) + 1.698\mathrm{Cos}(x_2)\mathrm{Sin}(x_2) - 0.2111\mathrm{Cos}(x_1)\mathrm{Cos}(x_2)\mathrm{Sin}(x_2) - 1.467\mathrm{Cos}(x_2)^2\mathrm{Sin}(x_2) + 5.109\mathrm{Sin}(x_1)\mathrm{Sin}(x_2) - 8.071\mathrm{Cos}(x_1)\mathrm{Sin}(x_1)\mathrm{Sin}(x_2) - 9.091\mathrm{Cos}(x_2)\mathrm{Sin}(x_1)\mathrm{Sin}(x_2) - 5.494\mathrm{Sin}(x_1)^2\mathrm{Sin}(x_2) + 5.08\mathrm{Sin}(x_2)^2 + 0.4327\mathrm{Cos}(x_1)\mathrm{Sin}(x_2)^2 - 0.7113\mathrm{Cos}(x_2)\mathrm{Sin}(x_2)^2 - 3.866\mathrm{Sin}(x_1)\mathrm{Sin}(x_2)^2 + 0.3384\mathrm{Sin}(x_2)^3$

Table 5 denotes the fitting and boundedness performance of mathematical models using to estimate ultimate tensile strength (UTS) of PP-based hybrid composites. According to results, sixth-order polynomial, second-order rational, and third-order trigonometric models show the best fitting performance in terms of R^2. However, rational and trigonometric models contain maximum and minimum values that cannot be encountered in practice. For this problem, ultimate tensile strength, which gives information about the material's resistance under tensile loading does not get a negative value. In addition to this, experimental results display that the minimum value of UTS is obtained as 16 MPa. Namely, the minimum strength value (7.38 MPa) obtained by model "SON" does not seem realistic. Because of all these reasons, the third-order multiple nonlinear model ("TON"), which has a more straightforward structure and produces more realistic values, is recommended in PP-based hybrid composite material design where strength is considered an important parameter.

Table 5. Fitting performance and boundedness of models for ultimate tensile strength

Model	R^2	Max.	Min.
TON	0.95	22.14	15.89
SON	1	30.66	7.38
SONR	1	22.34	-15.06
TOTN	1	28.98	-0.31

Figure 3 demonstrates a 3D plot of polynomial, rational and trigonometric models that best fit the experimental results concerning ultimate tensile strength. As mentioned above, graphical demonstration gives an essential idea to us concerning mathematical model selection. The rational model, which has many discontinuities and extreme values, is not suitable for expressing strength mathematically. It is decided that although the trigonometric model shows well fit with the experimental results, it is not a suitable model taking into account expert opinions. For similar reasons, "SON" model cannot be used either. In this regard, it can be said that the third order polynomial model is the most appropriate model that gives realistic results.

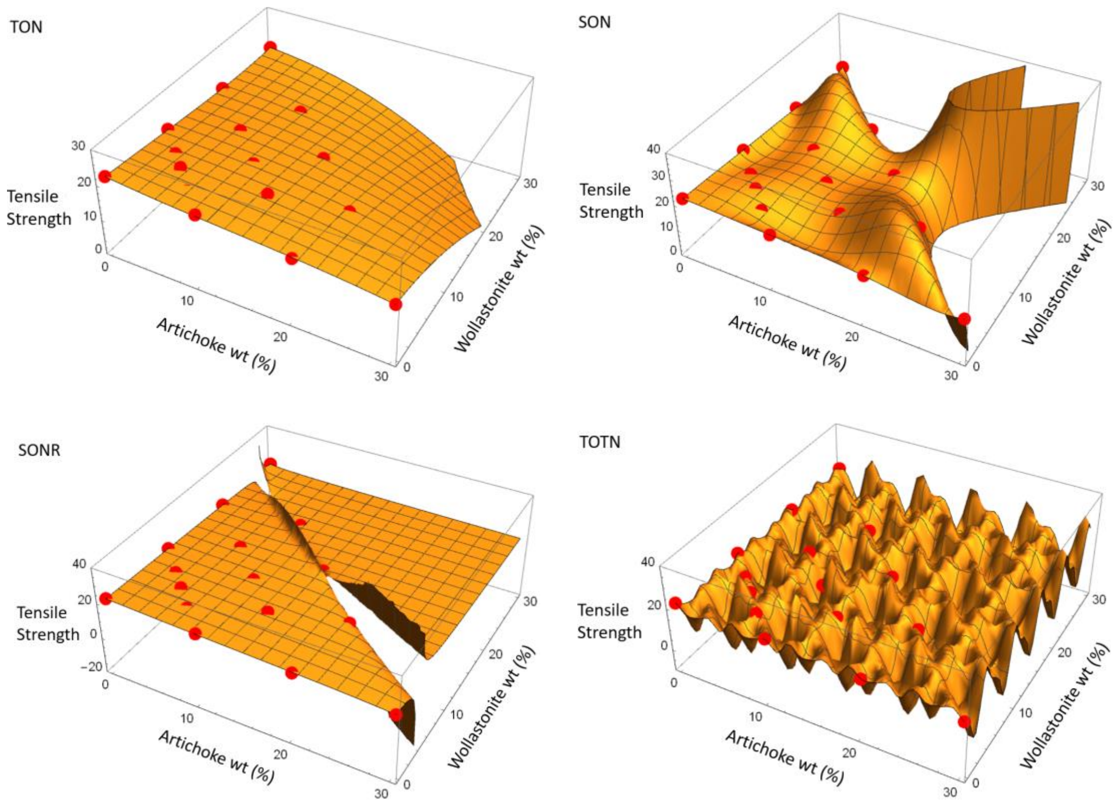

Figure 3. 3D plot representations of experimental data and recommended mathematical model for ultimate tensile strength

In order to define physical phenomena regarding the ultimate strain of PP-based hybrid composites, alternative four distinct mathematical models were given in Table 6.

Table 6. Mathematical Models for Ultimate Strain

Name	Models
Fourth order multiple nonlinear (FON)	$Y = 5.52 - 0.1943x_1 + 0.01213x_1^2 - 0.0005466x_1^3 + (8.891 \times 10^{-6})x_1^4 - 0.1006x_2 - 0.07173x_1x_2 + 0.006727x_1^2x_2 - 0.0001407x_1^3x_2 + 0.008007x_2^2 + 0.004726x_1x_2^2 - 0.0002343x_1^2x_2^2 - 0.000555x_2^3 - 0.00007394x_1x_2^3 + 0.00001102x_2^4$
Sixth order multiple nonlinear (SON)	$Y = 5.52 - 0.1422x_1 + 0.00196x_1^2 - 0.0004241x_1^3 + 0.00008384x_1^4 - (4.667 \times 10^{-6})x_1^5 + (7.816 \times 10^{-8})x_1^6 - 0.05474x_2 - 0.02993x_1x_2 + 0.007392x_1^2x_2 - 0.006162x_1^3x_2 + 0.0004825x_1^4x_2 - (9.539 \times 10^{-6})x_1^5x_2 - 0.001292x_2^2 - 0.002668x_1x_2^2 + 0.01165x_1^2x_2^2 - 0.0004904x_1^3x_2^2 + (8.529 \times 10^{-7})x_1^4x_2^2 - 0.0001888x_2^3 - 0.005781x_1x_2^3 - 0.0004778x_1^2x_2^3 + 0.00001849x_1^3x_2^3 + 0.00007167x_2^4 + 0.0004986x_1x_2^4 - (4.091 \times 10^{-8})x_1^2x_2^4 - (4.948 \times 10^{-6})x_2^5 - 0.00001018x_1x_2^5 + (9.358 \times 10^{-8})x_2^6$
Third order multiple nonlinear rational (TONR)	$Y = (-282.1 - 19300.x_1 - 51008.x_1^2 + 1498.x_1^3 - 22910.x_2 + 88659.x_1x_2 + 4026.x_1^2x_2 - 51201.x_2^2 - 839.8x_1x_2^2 + 4221.x_2^3)/(-51.15 + 40204.x_1 - 17431.x_1^2 + 463.2x_1^3 + 73167.x_2 - 3229.x_1x_2 + 2132.x_1^2x_2 - 23464.x_2^2 + 1371.x_1x_2^2 + 1388.x_2^3)$
Third order trigonometric multiple nonlinear (TOTN)	$Y = 0.921 + 0.2069\mathrm{Cos}(x_1) + 1.408\mathrm{Cos}(x_1)^2 + 0.3694\mathrm{Cos}(x_1)^3 + 0.1811\mathrm{Cos}(x_2) - 0.3544\mathrm{Cos}(x_1)\mathrm{Cos}(x_2) + 0.5762\mathrm{Cos}(x_1)^2\mathrm{Cos}(x_2) + 1.342\mathrm{Cos}(x_2)^2 + 0.5977\mathrm{Cos}(x_1)\mathrm{Cos}(x_2)^2 + 0.2719\mathrm{Cos}(x_2)^3 + 0.03054\mathrm{Sin}(x_1) + 0.5365\mathrm{Cos}(x_1)\mathrm{Sin}(x_1) - 0.406\mathrm{Cos}(x_1)^2\mathrm{Sin}(x_1) - 0.3352\mathrm{Cos}(x_2)\mathrm{Sin}(x_1) + 0.005495\mathrm{Cos}(x_1)\mathrm{Cos}(x_2)\mathrm{Sin}(x_1) + 0.237\mathrm{Cos}(x_2)^2\mathrm{Sin}(x_1) + 0.6831\mathrm{Sin}(x_1)^2 - 0.9424\mathrm{Cos}(x_1)\mathrm{Sin}(x_1)^2 - 0.1696\mathrm{Cos}(x_2)\mathrm{Sin}(x_1)^2 + 0.1425\mathrm{Sin}(x_1)^3 - 0.05898\mathrm{Sin}(x_2) - 0.4338\mathrm{Cos}(x_1)\mathrm{Sin}(x_2) + 0.2482\mathrm{Cos}(x_1)^2\mathrm{Sin}(x_2) + 0.6653\mathrm{Cos}(x_2)\mathrm{Sin}(x_2) + 0.4743\mathrm{Cos}(x_1)\mathrm{Cos}(x_2)\mathrm{Sin}(x_2) - 0.7262\mathrm{Cos}(x_2)^2\mathrm{Sin}(x_2) + 1.119\mathrm{Sin}(x_1)\mathrm{Sin}(x_2) - 0.7263\mathrm{Cos}(x_1)\mathrm{Sin}(x_1)\mathrm{Sin}(x_2) - 1.424\mathrm{Cos}(x_2)\mathrm{Sin}(x_1)\mathrm{Sin}(x_2) - 1.304\mathrm{Sin}(x_1)^2\mathrm{Sin}(x_2) + 0.803\mathrm{Sin}(x_2)^2 - 0.1215\mathrm{Cos}(x_1)\mathrm{Sin}(x_2)^2 - 0.3062\mathrm{Cos}(x_2)\mathrm{Sin}(x_2)^2 - 0.7467\mathrm{Sin}(x_1)\mathrm{Sin}(x_2)^2 + 0.07127\mathrm{Sin}(x_2)^3$

Table 7 denotes the fitting and boundedness performance of mathematical models using to estimate the ultimate strain of PP-based hybrid composites. Although it has a lower R^2 value as in models expressing elastic modulus and ultimate strength, the fourth-order polynomial model is the most appropriate model to explain the experimental results related to strain. Graphical representation in Figure 4 supports this idea.

Table 7. Fitting performance and boundedness of models for ultimate strain

Model	R^2	Max.	Min.
FON	0.95	5.52	2.70
SON	1	9.01	-0.53
TONR	1	36.58	-16.92
TOTN	1	5.82	-0.46

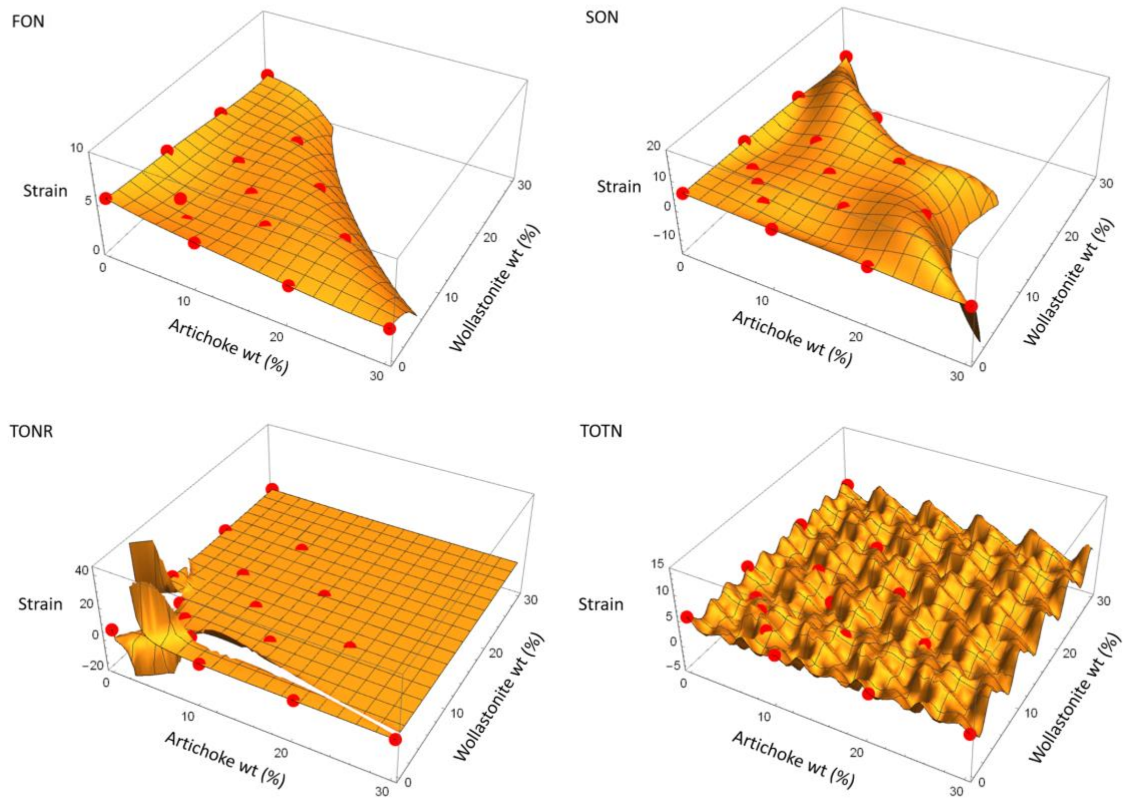

Figure 4. 3D plot representations of experimental data and recommended mathematical model for ultimate strain

5. Conclusions

In this study, artichoke stem particles and wollastonite were used as organic and inorganic fillers in order to improve the mechanical properties of polypropylene (PP). PP-based hybrid composites, including different proportions of artichoke stem particles and wollastonite, were mathematically modeled using the data regarding elastic modulus, ultimate strength, and strain obtained from the experimental study. The most critical parameter showing the usability of a mathematical model in the literature is the value of R^2. In this study, the primary purpose is to show that it is always possible to create a model with an R^2 value of 1. In this regard, 12 different polynomials, rational and trigonometric nonlinear models whose R^2 value is equal to 1 are given. However, a high value of R^2 itself does not always mean a good fit, and it does not define the entire physical phenomena of the engineering process. Graphically results given in the study denote that R^2 is not enough standalone criterion to evaluate the mathematical models. It has been specified that other criteria are needed to evaluate the models. It is impossible to obtain a realistic functional structure in cases where models are not examined in terms of stability. To overcome this drawback, by inspecting the boundedness of each candidate model the functions that produce value only within the physical limits have been admitted as successful. In the light of these evaluations, it was seen that only polynomial models fulfill the necessary success criteria.

Acknowledgments

The authors would like to thank KAOLIN Industrial Minerals for the wollastonite supply.

Author Statement

The authors confirm contribution to the paper as follows: study conception and design: Melih Savran; data collection: Mustafa Öncül, Kutlay Sever and Muhammed Yılmaz; analysis and interpretation of results: Kutlay Sever, Melih Savran, Mustafa Öncül, Muhammed Yılmaz; draft manuscript preparation: Melih Savran and Mustafa Öncül. All authors reviewed the results and approved the final version of the manuscript.

Conflict of Interest

The authors declare no conflict of interest.

References

Aktaş, L. T., & Aydın, L. (2021). Stochastic optimization and modeling of high-velocity impact tests on high-temperature carbon–carbon composites. *SN Applied Sciences*, *3*(3), 313. https://doi.org/10.1007/s42452-021-04321-0

Ashenai Ghasemi, F., Ghasemi, I., Menbari, S., Ayaz, M., & Ashori, A. (2016). Optimization of mechanical properties of polypropylene/talc/graphene composites using response surface methodology. *Polymer Testing*, *53*, 283–292. https://doi.org/10.1016/j.polymertesting.2016.06.012

Ayaz, M., Ghasemi, F. A., Rahimloo, V. P., & Menbari, S. (2018). Multi-response optimization of the mechanical properties of PP/talc/$CaCO_3$ ternary nanocomposites by the response surface methodology combined with desirability function approach. *Journal of Elastomers & Plastics*. https://doi.org/10.1177/0095244318819184

D20 Committee. (n.d.). *Test Method for Tensile Properties of Plastics*. ASTM International. https://doi.org/10.1520/D0638-14

Essabir, H., Nekhlaoui, S., Malha, M., Bensalah, M. O., Arrakhiz, F. Z., Qaiss, A., & Bouhfid, R. (2013). Bio-composites based on polypropylene reinforced with Almond Shells particles: Mechanical and thermal properties. *Materials & Design*, *51*, 225–230. https://doi.org/10.1016/j.matdes.2013.04.031

Guimarães, J. L., Frollini, E., da Silva, C. G., Wypych, F., & Satyanarayana, K. G. (2009). Characterization of banana, sugarcane bagasse and sponge gourd fibers of Brazil. *Industrial Crops and Products*, *30*(3), 407–415. https://doi.org/10.1016/j.indcrop.2009.07.013

Kaya, N., Atagur, M., Akyuz, O., Seki, Y., Sarikanat, M., Sutcu, M., Seydibeyoglu, M. O., & Sever, K. (2018). Fabrication and characterization of olive pomace filled PP composites. *Composites Part B: Engineering*, *150*, 277–283. https://doi.org/10.1016/j.compositesb.2017.08.017

Kılınc, A. C., Atagur, M., Ozdemir, O., Sen, I., Kucukdogan, N., Sever, K., Seydibeyoglu, O., Sarikanat, M., & Seki, Y. (2016). Manufacturing and characterization of vine stem reinforced high density polyethylene composites. *Composites Part B: Engineering*, *91*, 267–274. https://doi.org/10.1016/j.compositesb.2016.01.033

Mattos, B. D., Misso, A. L., de Cademartori, P. H. G., de Lima, E. A., Magalhães, W. L. E., & Gatto, D. A. (2014). Properties of polypropylene composites filled with a mixture of household waste of mate-tea and wood particles. *Construction and Building Materials*, *61*, 60–68. https://doi.org/10.1016/j.conbuildmat.2014.02.022

Mengeloglu, F., & Karakus, K. (2008). Thermal Degradation, Mechanical Properties and Morphology of Wheat Straw Flour Filled Recycled Thermoplastic Composites. *Sensors*, *8*(1), 500–519. https://doi.org/10.3390/s8010500

Nor, A. F. M., Hassan, M. Z., Rasid, Z. A., Aziz, S. A., Sarip, S., & Md Daud, M. Y. (2021). Optimization on Tensile Properties of Kenaf/Multi-walled CNT Hybrid Composites with Box-Behnken Design. *Applied Composite Materials*, *28*(3), 607–632. https://doi.org/10.1007/s10443-021-09879-x

Nourbakhsh, A., & Ashori, A. (2010). Wood plastic composites from agro-waste materials: Analysis of mechanical properties. *Bioresource Technology*, *101*(7), 2525–2528. https://doi.org/10.1016/j.biortech.2009.11.040

Polatoğlu, İ., Aydın, L., Nevruz, B. Ç., & Özer, S. (2020). A Novel Approach for the Optimal Design of a Biosensor. *Analytical Letters*, *53*(9), 1428–1445. https://doi.org/10.1080/00032719.2019.1709075

Ragunath, S., Shankar, A. N., Meena, K., Guruprasad, B., Madhu, S., Rakesh, N., Hariprabhu, M., Balamuralitharan, S., & Daniel, N. (2021). Multiobjective Optimization of Mechanical Properties on Sisal-Glass Fiber-Reinforced Hybrid Composites Using Response Surface Methodology and LINGO Analysis. *Advances in Materials Science and Engineering*, *2021*, 1–10. https://doi.org/10.1155/2021/2376148

Rong, M. Z., Zhang, M. Q., Liu, Y., Yang, G. C., & Zeng, H. M. (2001). The effect of fiber treatment on the mechanical properties of unidirectional sisal-reinforced epoxy composites. *Composites Science and Technology*, *61*(10), 1437–1447. https://doi.org/10.1016/S0266-3538(01)00046-X

Saba, N., Paridah, M. T., & Jawaid, M. (2015). Mechanical properties of kenaf fibre reinforced polymer composite: A review. *Construction and Building Materials*, *76*, 87–96. https://doi.org/10.1016/j.conbuildmat.2014.11.043

Sever, K., Sarikanat, M., Seki, Y., Erkan, G., Erdoğan, Ü. H., & Erden, S. (2012). Surface treatments of jute fabric: The influence of surface characteristics on jute fabrics and mechanical properties of jute/polyester composites. *Industrial Crops and Products*, *35*(1), 22–30. https://doi.org/10.1016/j.indcrop.2011.05.020

Sever, K., & Yılmaz, M. (2020). Evaluation of Mechanical and Thermal Properties of Artichoke Filled Polypropylene Composites: Influence of Wollastonite Hybridization. *Emerging Materials Research*, *9*(2), 1–6. https://doi.org/10.1680/jemmr.18.00121

Srivabut, C., Ratanawilai, T., & Hiziroglu, S. (2021). Statistical modeling and response surface optimization on natural weathering of wood–plastic composites with calcium carbonate filler. *Journal of Material Cycles and Waste Management*, *23*(4), 1503–1517. https://doi.org/10.1007/s10163-021-01230-7

Syed, S. F., Chen, J. C., & Guo, G. (2020). Optimization of Tensile Strength and Shrinkage of Talc-Filled Polypropylene as a Packaging Material in Injection Molding. *Journal of Packaging Technology and Research*, *4*(1), 69–78. https://doi.org/10.1007/s41783-019-00077-6

Verma, D., & Gope, P. C. (2015). The use of coir/coconut fibers as reinforcements in composites. In *Biofiber Reinforcements in Composite Materials* (pp. 285–319). Elsevier. https://doi.org/10.1533/9781782421276.3.285

Xu, Y., Wu, Q., Lei, Y., & Yao, F. (2010). Creep behavior of bagasse fiber reinforced polymer composites. *Bioresource Technology*, *101*(9), 3280–3286. https://doi.org/10.1016/j.biortech.2009.12.072

Yao, F., Wu, Q., Lei, Y., & Xu, Y. (2008). Rice straw fiber-reinforced high-density polyethylene composite: Effect of fiber type and loading. *Industrial Crops and Products*, *28*(1), 63–72. https://doi.org/10.1016/j.indcrop.2008.01.007

Yiga, V. A., Lubwama, M., Pagel, S., Olupot, P. W., Benz, J., & Bonten, C. (2021). Optimization of tensile strength of PLA/clay/rice husk composites using Box-Behnken design. *Biomass Conversion and Biorefinery*. https://doi.org/10.1007/s13399-021-01971-3

Scientific Research Communications

Research Article

Sci. Res. Comm. (2022)
Volume 2, Issue 1
doi: 10.52460/src.2022.003

Quantification of Afghan Saffron's Moisture and Main Compounds (Crocin, Picrocrocin and Safranal) for Quality Evaluation

Raihana Halim[1,2]*, Najia Sherzay[1,3], Nazifa Faqeryar[4], M. Homayoun Hashimi[1]

[1] Department of Biochemistry, Faculty of Pharmacy, Kabul University, Kabul, Afghanistan
[2] Department of Biotechnology, Institute of Natural Science, Çukurova University, Adana, Turkey
[3] Institute of Pathology, Laboratory and Forensic Medicine (I-PPerForM), Universiti Teknologi MARA, 47000, Sungai Buloh, Selangor, Malaysia
[4] Avignon University, INRAE, UMR408, GREEN Extraction Team, 84000, Avignon, France
*Corresponding author: halimraihana@gmail.com

Received: 17.12.2021 Accepted: 27.01.2022

Abstract

Saffron, the stigmas of the plant *Crocus sativus* L., has attracted the worldwide interest for its specific organoleptic and pharmacological characteristics. Cultivation of saffron in Afghanistan began in recent years and in very short time Afghan saffron hit higher record. Till now, there is no scientific study which has analyzed its characteristics according to ISO methods. In this study, the main components of Afghan saffron have been described, and quality parameters along with its characteristics were analyzed according to ISO-3632-2 test methods. The results of moisture analysis (5.12 to 5.74%) and determination of crocin (230.52-255.15) of Afghan saffron were at the range of standard as described for category I of saffron in ISO 3632-2 test methods. However, the results of some samples for safranal and picrocrocin (38.52-40.21 for safranal and 68.86-72.63 for picrocrocin) were higher than the range of category I of ISO 3632-2.

Keywords: Afghans saffron, moisture, bioactive compounds, ISO 3632-2

1. Introduction

Saffron, the plant *Crocus sativus* L., is a member of the family *Iridaceae*; the dried stigmas of this plant with dark red color and trumpet-shaped are some of the world's most expensive spices (Jan et al., 2014). Few spices can provide a combination of color, taste, and aroma and the most popular of these is saffron (García-Rodríguez et al., 2014).

In ancient times, saffron was mainly used for dyeing such as dyeing silk and other textiles, and it is still used as a cosmetic and food colorant (Tsatsaroni & Eleftheriadis, 2008), but recent studies have also concentrated on its medical properties such as, antidepressant, antispasmodic, antidiabetic, anticancer, aphrodisiac and expectorant (Abdullaev, 2002; Manzo et al., 2015; Sereshti et al., 2014; Jan et al., 2014; Melnyk et al., 2010; Sanchez et al., 2008). Saffron contains more than 150 volatile and non-volatile components (Padmavathy et al., 2011), but three major bioactive compounds of saffron are crocin, picrocrocin (Gikas et al., 2021) and safranal which are responsible for color, taste, and aroma, respectively; and saffron's quality depends on the concentration of these three main metabolites (Kiani et al., 2018; Sanchez et al., 2009; Sujata et al., 1992). Crocins are water-soluble carotenoid compounds related to the mono- and di-glycosyl esters of polyene dicarboxylic acid (Lozano et al., 1999) which have shown to improve memory (Pitsikas et al., 2007), improve autoimmune disease, antioxidant, anti-inflammatory (Korani et al., 2019), and antidepressant activities (Lee et al., 2015; Wang et al., 2010). Picrocrocin ($C_{16}H_{26}O_7$) is considered to be the main bitter principle of saffron. It is a monoterpene glycoside precursor of safranal (Lage & Cantrell, 2009). Safranal is mainly an essential oil and is responsible for the odor of saffron. Chemically it is monoterpene aldehyde ($C_{10}H_{14}O$) which is formed during the drying and storage of the hydrolysis of picrocrocin. It is believed that this bioactive compound of saffron is responsible for its antioxidant, anticonvulsant, hypnotic, and anti-cancer effects (Chaudhari et al., 2013). These three metabolites are among the most important chemical factors in evaluating the nutritional and pharmacological quality of saffron (Bolandi et al., 2004; Zalacain et al., 2005; Zougagh, 2006). The moisture content of a food is dependent on species, variety, maturity of food and the relative humidity of the environment (Gazor & Chaji, 2010). Therefore, the most important factors that affect the quality of the saffron during storage and can cause degradation and reduction of its quality are the product's moisture, relative humidity, ambient temperature, storage and light (Bolandi et al., 2004).

Global consumers of saffron give high importance to saffron's quality because on one hand, the quality can affect consumers' health (Sereshti et al., 2018), and on the other hand, due to its high price, it is susceptible to fraudulent practices (Petrakis & Polissiou, 2017; Kiani et al., 2018).

These valuable plant species are cultivated in environments with very different climatic conditions and are well adapted to arid and semi-arid lands which produce stigmas annually. It is also adaptable to temperate and sub-tropical climates and can be grown on soils varying from sandy to well-drained clay loams (Isfahani et al., 2013; Lage & Cantrell, 2009). Therefore, saffron is well suited to conditions in eastern Afghanistan, so it plays a major role in the country's socio-economical development (Peter, 2007).

Afghan saffron is a sustainable substitute crop with high value in some agricultural areas of Afghanistan for socio-economical development. Afghanistan is the 4th saffron producer in the world by producing significant amounts per year (average amount of 4 tons). In addition, Afghan saffron is the winner of the Superior Taste Awards from the International Taste & Quality Institute- Brussels (Katawazy, 2013). Despite all these, Afghan saffron's characteristics are not well recognized, because there is not any written and published proof of its quality according to ISO standards. Even Afghanistan is not on the list of saffron-producing countries. Hence, this study aimed to analyze the quality parameters for Afghan saffron. If Afghan saffron is recognized as special because of its quality, producers could ask for more than buyers pay for saffron from other countries. To the best of the authors' knowledge, this is the first study that has evaluated the most important characteristics of Afghan saffron according to ISO-3632-2 (2011).

2. Methodology

Five samples (S1, S2, S3, S4, S5) were obtained from different wholesale saffron suppliers of Herat city with a guarantee of being free from adulteration on March 2019. The sampling was carried out according to the method described in ISO 948 and the samples were stored at 4 °C in the dark until the analysis was performed. Plastic bags were used for the packaging of saffron samples. All other necessary chemical reagents and some apparatus were supplied from chemical supplying companies in Kabul city. The samples were coded from 1 to 5 instead of using the names of the suppliers. The moisture content and main compounds of saffron (crocin, picrocrocin and safranal) determination were performed as indicated in ISO 3632-2 for quality evaluation of Afghan saffron. All tests were performed on samples from September to November 2019.

Quality evaluation of saffron moisture and volatile matter content

Moisture and volatile matter content is expressed as a percentage mass fraction of the sample. The test is performed as per ISO 3632-2. Around 2.5 g of the sample was weighed into the weighing dish. The uncovered weighing dish was placed into the oven maintained at 103 °C and left for 16 h. Then it was covered with a lid, and allowed to cool in the desiccator. After cooling, samples were weighed again to find the change in the moisture content. The test was performed two times for each sample and the average amount was used for analyzing test results.

The moisture and volatile matter content, W_{MV}, expressed as a percentage of the initial sample in Equation (1):

$$W_{MV} = (m_0 - m_4) \times \frac{100}{m_0} \% \quad (1)$$

where

m_0 is the mass, in grams, of the test portion;

m_4 is the mass, in grams, of the dry residue.

Quality evaluation of saffron by determining the main characteristics

Tree main bioactive compounds of saffron, namely safranal, crocin and picrocrocin were analyzed in accordance with the spectrometric test method given in ISO 3632-2. Spectrophotometric assays were carried out with Shimadzu UV-1800 UV-Vis spectrophotometer (Shimadzu, Kyoto, Japan) using quartz cells of 1 cm path length. Absorbances were recorded between 200-700nm using the “photometric” function. All measurements were taken at room temperature.

Saffron stigmata were ground in a glass mortar and pestle. The ground saffron was passed through a 0.5 mm mesh. 500 mg of ground saffron was transferred to a 1000 ml balloon and 500 ml of distilled water was added and mixed well. The mixture was agitated by magnetic stirrer for one hour in the dark. The volume was completed to 1L with distilled water. 20 ml of the mentioned solution was transferred to a 200 ml balloon, and the volume was completed with the distilled water. The solution was then filtered by a membrane filter with a pore diameter of 0.45 µ.

The absorbance of the prepared solutions of all samples was evaluated at a wavelength of 330, 440, and 257nm for safranal, crocin, and picrocrocin; respectively. The spectrum of saffron in aqueous solution is illustrated in Figure 1 to show the peaks for safranal, crocin and picrocrocin at 200 -700 nm range.

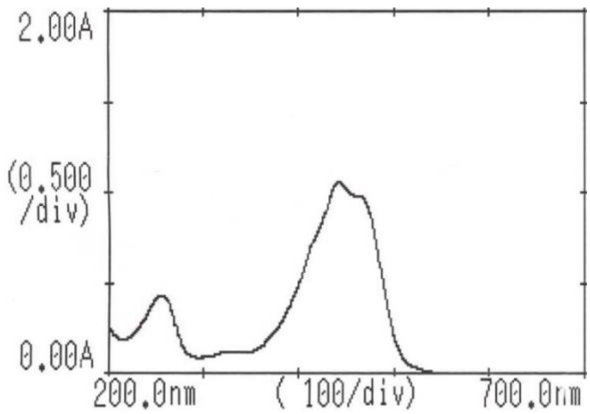

Figure 1. Spectrum of Afghan saffron in aqueous solution showing the peaks for safranal, crocin and picrocrocin at 200 -700 nm range

Statistical analysis

Data were analyzed using GraphPad Prism 5.0 and results were expressed as mean and ± SD.

3. Results and Discussion

Moisture and volatile matter content test results

The moisture content of saffron samples in our research ranged from 5.12 to 5.74% (Table 1). According to ISO-3632-2, the moisture content for Grade I should be less than 10%; therefore, the percentage moisture and volatile matter content of Afghan saffron is in the range of Grade I. The moisture content of Grade I saffron from Greece was determined to be ranging from 5.49% to 9.96% (Maggi et al., 2011), the moisture content of Grade I saffron from Italy ranged from 5.35% to 8.79% (Giorgi et al., 2017); and for Grade I Spanish saffron the volatile contents were 5.49% to 10.43% (García-Rodríguez et al., 2017). According to another study (Azarabadi & Özdemir, 2018), the moisture content of Iranian samples differed from 4.96% to 6.13%.

Bioactive compounds

In all of our samples the results for bioactive compounds were between 230.52-255.15 for crocin, 38.52-40.21 for safranal, and 68.86-72.63 for picrocrocin; which are in the standard range according to the ISO-3632-2. In previous studies, the safranal content for Italian saffron were measured from 23.2 to 49 (Manzo et al., 2015); according to the research performed by García-Rodríguez et al., (2017) the safranal content of Greece saffron ranged between 29.81-45.55; safranal quantity of Iranian Grade I Saffron ranged between 30.00-43.64; safranal quantity in Spanish Saffron was between 28.58-46.07; and safranal quantity of Italian saffron ranged between 28.58-46.07. According to a study performed by Azarabadi and Özdemir (2018), the crocin amount of Iranian saffron was between 51.66 - 66.67 mg/g (Azarabadi & Ozdemir, 2018). The highest crocin amount of Italian saffron was 234.90 (Manzo et al., 2015). Regarding the results of our study, the highest crocin amount of Afghan saffron is 255.15 which indicates the highest quality of Afghan saffron. As a result of another study, the picrocrocin amount of Italian saffron ranged from 81.30 to 113.00 which is close to Afghan saffron picrocrocin value. The high values of picrocrocin in Afghan saffron give the unique property to Afghan saffron worldwide. The values are presented in Table 2.

Table 1. The quality parameters of Afghan saffron

Sample ID	Moisture & volatile contents (%)	Bioactive compounds		
		Crocin	Safranal	Picrocrocin
S1	5.45	230.52	39.52	72.61
S2	5.51	246.73	40.21	71.15
S3	5.12	234.10	39.15	70.10
S4	5.74	247.36	39.27	68.86
S5	5.21	255.15	38.52	72.63
Mean	5.406	242.772	39.334	71.07
Standard Deviation	0.247245	10.18879	0.612887	1.63069

Table 2. Comparison of quality parameters of saffron from different countries

Origin country	Moisture & volatile contents (%)	Bioactive compounds		
		Crocin	Safranal	Picrocrocin
Greece	5.49 – 9.96		29.81 - 45.55	
Italy	5.35 – 8.79	max. 234.90	23.2 – 49.00	81.30 - 113.00
Spain	5.49 – 10.43		28.58 - 46.07	
Iran	4.96 – 6.13	51.66 - 66.67	30.00 - 43.64	
Afghan	5.12 – 5.74	230.52 – 255.15	38.52 – 40.21	68.86 – 72.63

4. Conclusions

Afghan Grade I saffron moisture and bioactive compounds has met all of the Grade I saffron characteristics of ISO 3632-2 test methods, with high flavoring and coloring strength due to the bioactive compounds. It has also proved that the region is most suitable for the cultivation of saffron therefore is a good choice for Afghan farmers to cultivate it. The results of the analysis of most samples show that Afghan saffron has high quality; however, this study is not sufficient and further research is needed. In order to be able to provide a separate identity for Afghan saffron, all other quality determination tests should be performed according to ISO 3632-2 methods.

Acknowledgments

The authors would like to thank the HEDP and World Bank for its financial support of this project.

Author Statement

The authors confirm contribution to the paper as follows: study conception and design: Raihana Halim, Najia Sherzay, Nazifa Faqeryar; data collection: Raihana Halim, Najia Sherzay, M. Homayoun Hashimi; analysis and interpretation of results: Raihana Halim, Najia Sherzay; draft manuscript preparation: Raihana Halim, Najia Sherzay, and Nazifa Faqeryar. All authors reviewed the results and approved the final version of the manuscript.

Conflict of Interest

Example: The authors declare no conflict of interest.

References

Abdullaev, F. I. (2002). Cancer Chemopreventive and Tumoricidal Properties of Saffron (Crocus sativus L.). *Experimental Biology and Medicine, 227*(1), 20-25. doi: 10.1177/153537020222700104

Azarabadi, N., & Özdemir, F. (2018). Determination of Crocin Content and Volatile Components in Different Qualities of Iranian Saffron. *Gıda / The Journal of Food*, 43(3), 476-489. doi.org/10.15237/gida.GD18018

Bolandi, M., Amin, L. M., Karbassi, A., Ghodousi, H. B., & Mesbahi, G. (2004). Effect of Drying Methods and Light on the Cemical Characteristics of Saffron (Crocus Sativus L.) During storage. *Agricultural Sciences and Technology*, 18(2), 197-204.

Chaudhari, S. P., Bhandurge, N. B., Ratnaparkhi, M. P. (2013). Development and validation of UV spectrophotometric method of safranal. *Pelagia Research Library*. 4(4), 136-140.

García-Rodríguez, M. V., López-Córcoles, H., Alonso, G. L., Pappas, C. S., Polissiou, M. G., & Tarantilis, P. A. (2017). Comparative evaluation of an ISO 3632 method and an HPLC-DAD method for safranal quantity determination in saffron. *Food Chemistry,* 221, 838-843. https://doi.org/10.1016/j.foodchem.2016.11.089

García-Rodríguez, M. V., Serrano-Diaz, J., Tarantilis, P. A., López-Córcoles, H., Carmona, M., Alonso, G. L. (2014). Determination of Saffron Quality by High-Performance Liquid Chromatography. *Journal of Agricultural and Food Chemistry,* 62(32), 8068-8074. https://doi.org/10.1021/jf5019356

Gazor, H. R., Chaji, H. (2010). Equilibrium moisture content and heat of desorption of saffron. *International Journal of Food Science & Technology,* 45(8), 1703-1709. https://doi.org/10.1111/j.1365-2621.2010.02321.x

Gikas, E., Koulakiotis, N. S., Tsarbopoulos, A. (2021). Phytochemical Differentiation of Saffron (Crocus sativus L.) by High Resolution Mass Spectrometry Metabolomic Studies. *Molecules,* 26(8), 2180. https://doi.org/10.3390/molecules26082180

Giorgi, A., Pentimalli, D., Giupponi, L., Panseri, S. (2017). Quality traits of saffron (*Crocus sativus* L.) produced in the Italian Alps. *Open Agriculture,* 2(1), 52-57. https://doi.org/10.1515/opag-2017-0005

Isfahani S. M. M., et al. (2013). Concentration of crocin, picrocrocin and safranal in Crocus sativus L. under different methyl jasmonate treatment. *Technical Journal of Engineering and Applied Sciences*, 3669-3673.

Jan, S., Wani, A., Kamili, A. N., Kashtwari, M. (2014). Distribution, chemical composition and medicinal importance of saffron (Crocus sativus L.). *African Journal of Plant Science*, 8(12), 537-545.

Katawazy, A. S. (2013). *A Comprehensive Study of Afghan Saffron*. Report of Research, Planning and Policy Directorate, Afghanistan Investment Support Agency.

Kiani, S., Minaei, S., Ghasemi-Varnamkhasti M. (2018). Instrumental approaches and innovative systems for saffron quality assessment. *Journal of Food Engineering*. 216, 1-10. https://doi.org/10.1016/j.jfoodeng.2017.06.022

Korani, S., Korani, M., Sathyapalan, T., Sahebkar, A. (2019). Therapeutic effects of Crocin in autoimmune diseases: A review. *BioFactors, 45*(6), 835-843. https://doi.org/10.1002/biof.1557

Lage, M., Cantrell, C. L. (2009). Quantification of saffron (Crocus sativus L.) metabolites crocins, picrocrocin and safranal for quality determination of the spice grown under different environmental Moroccan conditions. *Scientia Horticulturae*, 121(3), 366–373. https://doi.org/10.1016/j.scienta.2009.02.017

Lee, F. Y., Htar, T. T., Akowuah, G. A. (2015). ATR-FTIR and Spectrometric Methods for the Assay of Crocin in Commercial Saffron Spices (*Crocus savitus* L.). *International Journal of Food Properties,* 18(8), 1773-1783. doi:10.1080/10942912.2014.923911

Lozano, P., Castellar, M. R., Simancas, M. J., Iborra, J. (1999). A quantitative high-performance liquid chromatographic method to analyse commercial saffron (*Crocus sativus* L.) products. *Journal of Chromatography A,* 830(2), 477-483. https://doi.org/10.1016/S0021-9673(98)00938-8

Maggi, L., Sanchez A. M, Carmona, M., et al. (2011). Rapid determination of safranal in the quality control of saffron spice (*Crocus sativus* L.). *Food Chemistry*, 127(1), 369–373. https://doi.org/10.1016/j.foodchem.2011.01.028

Manzo, A., Panseri, S., Bertoni, D., Giorgi, A. (2015). Economic and Qualitative Traits of Italian Alps Saffron. *Journal of Mountain Science*, 12, 1542-1550. doi: 10.1007/s11629-015-3448-3

Melnyk, J. P., Wang, S., Marcone, M. F. (2010). Chemical and biological properties of the world's most expensive spice: Saffron. *Food Research International*, 43(8), 1981–1989. https://doi.org/10.1016/j.foodres.2010.07.033

Padmavathy, J., Kumar, C. P., Saraswathi, S., et al. (2011). Pharmacological, Pharmacognostic and Phytochemical Review of Saffron. *International Journal of Pharmacy & Technology*, 3(3), 1214-1234.

Peter, W. (2007). Marketing Afghan Saffron. *International Research and Development,* Washington State University.

Petrakis, E. A., Polissiou, M. G. (2017). Assessing saffron (*Crocus sativus* L.) adulteration with plant-derived adulterants by diffuse reflectance infrared Fourier transform spectroscopy coupled with chemometrics. *Talanta*, 162, 558-566. https://doi.org/10.1016/j.talanta.2016.10.072

Pitsikas, N., Zisopoulou, S., Tarantilis, P. A., Kanakis, C. D., Polissiou, M. G., Sakellaridis, N. (2007). Effects of the active constituents of *Crocus sativus* L., crocins on recognition and spatial rats' memory. *Behavioural Brain Research,* 183(2), 141-146. https://doi.org/10.1016/j.bbr.2007.06.001

Sanchez, A. M., Carmona, M., del Campo, C. P., Alonso, G. L. (2009). Solid-phase Extraction for Picrocrocin Determination in the Quality Control of Saffron Spice (*Crocus sativus* L.). *Food Chemistry*, 116(3), 792-798. doi: 10.1016/j.foodchem.2009.03.039

Sanchez, A. M., Carmona, M., Zalacain, A., et al. (2008). Rapid Determination of Crocetin Esters and Picrocrocin from Saffron Spice (*Crocus sativus* L.) using UV–Visible Spectrophotometry for Quality Control. *Journal of Agricultural and Food Chemistry*, 56(9), 3167–3175. https://doi.org/10.1021/jf703725e

Sereshti, H., Heidari R., Samadi, S. (2014). Determination of volatile components of saffron by optimized ultrasound-assisted extraction in tandem with dispersive liquid-liquid microextraction followed by gas chromatography-mass spectrometry. *Food Chemistry*, 143, 499-505. https://doi.org/10.1016/j.foodchem.2013.08.024

Sereshti, H., Poursorkh, Z., Aliakbarzadeh, G., et al. (2018). An image analysis of TLC patterns for quality control of saffron based on soil salinity effect: A strategy for data (pre)-processing. *Food Chemistry*, 239, 831–839. https://doi.org/10.1016/j.foodchem.2017.07.012

Sujata V., Ravishankar, G. A., Venkataraman, L. V. (1992). Methods for the analysis of the saffron metabolites crocin, crocetins, picrocrocin and safranal for the determination of the quality of the spice using thin-layer chromatography, high-performance liquid chromatography and gas chromatography. *Journal of Chromatography*, 624(1-2), 497-502. https://doi.org/10.1016/0021-9673(92)85699-T

Tsatsaroni, E. G., Eleftheriadis, I. C. (2008). The colour and fastness of natural saffron. *Journal of the Society of Dyers and Colourists*, 110(9), 313-315. doi:10.1111/j.1478-4408.1994.tb01666.x

Wang, Y., Han, T., Zhu, Y., Zheng, C.-J., Ming, Q.-L., Rahman, K., Qin, L.-P. (2010). Antidepressant properties of bioactive fractions from the extract of *Crocus sativus* L. *Journal of Natural Medicines,* 64, 24. https://doi.org/10.1007/s11418-009-0360-6

Zalacain, A., Ordoudi, S. A., Díaz-Plaza, E. M., Carmona, M., Blázquez, I., Tsimidou, M. Z., Alonso, G. L. (2005). Near-infrared spectroscopy in saffron quality control: Determination of chemical composition and geographical origin. *Journal of Agricultural and Food Chemistry,* 53(24), 9337-9341. https://doi.org/10.1021/jf050846s

Zougagh, M., Rios, A., Valcarcel, M. (2006). Determination of total safranal by *in situ* acid hydrolysis in supercritical fluid media: Application to the quality control of commercial saffron. *Analytica Chimica Acta*, 578(2), 117–121. https://doi.org/10.1016/j.aca.2006.06.064

Scientific Research Communications

Research Article

Sci. Res. Comm. (2022)

Volume 2, Issue 1

doi: 10.52460/src.2022.004

Charlier Series Solutions of Systems of First Order Delay Differential Equations with Proportional and Constant Arguments

Ömür Kıvanç Kürkçü[1,*], Mehmet Sezer[2]

[1] Department of Engineering Basic Sciences, Konya Technical University, Konya, Turkey
[2] Department of Mathematics, Manisa Celal Bayar University, Manisa, Turkey
*Corresponding author: omurkivanc@outlook.com

Received: 31.10.2021 Accepted: 27.01.2022

Abstract

This study is devoted to obtaining the Charlier series solutions of first order delay differential equations involving proportional and constant arguments by employing an inventive numerical method dependent upon a collaboration of matrix structures derived from the parametric Charlier polynomial. The method essentially conducts the conversion of the unknown terms into a unique matrix equation at the collocation points, which yields a direct computation for these stiff equations. Two illustrative examples are included to test the accuracy and efficiency of the method. According to the investigation of the graphical and numerical results, the method holds fast, inventive and accurate computation, regularizing the matrix forms in compliance with the equations in question.

Keywords: Charlier polynomial, Collocation points, Delay arguments, Matrix method

1. Introduction

In this paper, the main aim is focused on obtaining the Charlier series solutions of the systems of the delay differential equations involving proportional and constant arguments (SDDEs) in the form

$$\sum_{k=0}^{1}\sum_{j=1}^{2}\left(P_{ij}^{k}(x)\,y_j^{(k)}(x)+Q_{ij}^{k}(x)\,y_j^{(k)}\left(\alpha_{jk}x+\beta_{jk}\right)\right)=g_i(x),\quad i=1,2, \tag{1}$$

on [a,b], subject to the initial conditions $y_i(a)=\lambda_i$. Here, $P_{ij}^{k}(x)$, $Q_{ij}^{k}(x)$ and $g_i(x)$ are continuous functions; α_{jk} and β_{jk} are proportional and constant delay arguments $\left(\alpha_{jk}\in(0,1],\beta_{jk}\in[-1,1]/\{0\}\right)$, respectively. The Charlier series solutions are extracted by the parametric Charlier polynomial, as

$$y_i(x)\cong\sum_{n=0}^{N}a_{in}C_n(x,\alpha),\quad \alpha>0, \tag{2}$$

where a_{in}'s are unknown Charlier coefficients to be released by the method and $C_n(x,\alpha)$ implies the Charlier polynomials with the parameter α.

As a special form of SDEs, the systems of differential equations with time delays (SDDEs) are of great importance in the modelling of population dynamics, such as predator-prey systems, and HIV infection of $CD4^{+}$ T-cells (Gokmen et al., 2015; Culshaw and Ruan, 2000; Kuang, 1993; Cushing, 1977). Recently, these type systems also continue to undergo the sustainable development for specific models, such as drug therapy for HIV infection via the system of fractional differential equations (Thirumalai et al., 2021). It is acceptable to express that the analytical solutions of SDEs are barely obtained via any analytical procedure. Thus, some efficient numerical methods are prepared to consider this issue. So far, a Chebyshev polynomial method has been proposed for the systems of higher order differential equations (Akyüz and Sezer, 2003). The Taylor collocation method has been used for linear differential-difference equations (Gökmen and Sezer, 2013). He's variational iteration method has been employed for solving the systems of differential equations (Tatari and Dehghan, 2009). The exponential Galerkin method and the optimal perturbation iteration method have been proposed for treating a HIV infection model of $CD4^{+}$ T-cells (Yüzbaşı and Karaçayır, 2017; Deniz, 2021). The optimal perturbation iteration method has also been applied to approach to the solution of a fractional Ebola virus disease model (Srivastava and Deniz, 2021). The Adomian decomposition method has been utilized to solve the continuous population models for single and interacting species (Pamuk, 2005). The differential transformation method has been utilized to obtain the solutions of systems of differential equations (Abdel-Halim Hassan, 2008).

Having been motivated by the studies above, this study deals with an inventive numerical method based on the Charlier polynomials to readily solve SDDEs, collaborating the matrix expansions with regard to the terms in Eq. (1).

This study is organized as follows: Section 2 reveals some properties of the Charlier polynomials. Section 3 comprises the method of solution via the collaboration of the matrices. Section 4 processes two numerical examples to exhibit the accuracy and efficiency of the present method. Section 5 discusses the innovations and outcomes, which are produced by the method presented in Section 4.

2. Some properties of Charlier polynomials

The discrete Charlier polynomials can be given by the generating function, as (Dunster, 2001; Szegö, 1975)

$$\sum_{n=0}^{\infty} C_n(x,\alpha)\frac{z^n}{n!} = \frac{(1+z)^x}{e^{\alpha z}},$$

and their explicit formulation can also be of the form (Dunster, 2001; Szegö, 1975)

$$C_n(x,\alpha) = \sum_{k=0}^{n} k!\binom{n}{k}\binom{x}{k}(-\alpha)^{n-k}.$$

They govern a discrete orthogonality relation stemmed from the Poisson distribution (Roman, 1984; Dunster, 2001)

$$\sum_{k=0}^{\infty} C_m(k,\alpha)C_n(k,\alpha)w(k) = \alpha^n n!\delta_{mn},\ \alpha>0,$$

subject to the Poisson density $w(k)=\alpha^k/(e^{\alpha}k!)$ in terms of the parameter α.

These polynomials possess a recurrence relation (Dunster, 2001)

$$C_{n+1}(x,\alpha)=(x-n-\alpha)C_n(x,\alpha)-\alpha n C_{n-1}(x,\alpha).$$

On the other hand, the uniform asymptotic expansions of the Charlier polynomials were discussed in (Dunster, 2001). The uniform and non-uniform asymptotics of the Charlier polynomials were studied using difference equation methods in (Huang et al., 2021). The Szász type operators composed of the Charlier polynomials were derived in (Varma and Taşdelen, 2012).

3. Method of solution: A collaboration of matrices

In this section, the method is established via the matrices of the terms in Eq. (1) and their collaboration structure via the Charlier polynomials. First, by the Charlier series solution form (2), its matrix relation turns out to be

$$y_i(x)=\boldsymbol{C}(x,\alpha)\boldsymbol{A}_i=\boldsymbol{\chi}(x)\boldsymbol{L}(\alpha)\boldsymbol{A}_i,\ i=1,2, \tag{3}$$

where

$$\boldsymbol{C}(x,\alpha)=\begin{bmatrix}C_0(x,\alpha) & C_1(x,\alpha) & \cdots & C_N(x,\alpha)\end{bmatrix},\ \boldsymbol{\chi}(x)=\begin{bmatrix}\binom{x}{0} & \binom{x}{1} & \cdots & \binom{x}{N}\end{bmatrix},$$

$$\boldsymbol{A}_i=\begin{bmatrix}a_{i0} & a_{i1} & \cdots & a_{iN}\end{bmatrix}^T,$$

and

$$\boldsymbol{L}^T(\alpha)=\begin{bmatrix} l_{00}(\alpha) & 0 & 0 & \cdots & 0\\ l_{10}(\alpha) & l_{11}(\alpha) & 0 & \cdots & 0\\ l_{20}(\alpha) & l_{21}(\alpha) & l_{22}(\alpha) & \cdots & 0\\ \vdots & \vdots & \vdots & \ddots & \vdots\\ l_{N0}(\alpha) & l_{N1}(\alpha) & l_{N2}(\alpha) & \cdots & l_{NN}(\alpha)\end{bmatrix},$$

such that

$$l_{mn}(\alpha)=\begin{cases} n!\binom{m}{n}(-\alpha)^{m-n}, & m\ge n\\ 0 & m<n\end{cases},\ m,n=0,1,\ldots,N.$$

It is obvious that the matrix relation (3) is not ready to be involved in the method since it is composed of non-smooth polynomial expansion. An inventive transitive matrix relation is thus, deployed as follows:

Theorem 3.1. Let $s(n,k)$, $\boldsymbol{S}_1$ and $\boldsymbol{X}(x)$ be the Stirling number of the first kind, a upper triangular matrix and a Taylor polynomial base, respectively. Then, a transitive matrix relation is constructed as

$$\boldsymbol{\chi}(x)=\boldsymbol{X}(x)\boldsymbol{S}_1, \tag{4}$$

where

$$\boldsymbol{X}(x)=\begin{bmatrix}1 & x & \cdots & x^N\end{bmatrix} \text{ and } \boldsymbol{S}_1=\begin{bmatrix}\frac{s(0,0)}{0!} & \frac{s(1,0)}{1!} & \frac{s(2,0)}{2!} & \cdots & \frac{s(N,0)}{N!} \\ 0 & \frac{s(1,1)}{1!} & \frac{s(2,1)}{2!} & \cdots & \frac{s(N,1)}{N!} \\ 0 & 0 & \frac{s(2,2)}{2!} & \cdots & \frac{s(N,2)}{N!} \\ \vdots & \vdots & \vdots & \ddots & \vdots \\ 0 & 0 & 0 & \cdots & \frac{s(N,N)}{N!}\end{bmatrix}.$$

Proof. By making use of a combinatorial property, which is presented in (Butzer et al., 1989), as

$$\binom{x}{n}=\sum_{k=0}^{n}\frac{s(n,k)x^k}{n!},$$

it can be expanded via the matrix relations, as

$$\underbrace{\begin{bmatrix}\binom{x}{0} \\ \binom{x}{1} \\ \binom{x}{2} \\ \vdots \\ \binom{x}{N}\end{bmatrix}}_{\boldsymbol{\chi}^T(x)}=\underbrace{\begin{bmatrix}\frac{s(0,0)}{0!} & 0 & 0 & \cdots & 0 \\ \frac{s(1,0)}{1!} & \frac{s(1,1)}{1!} & 0 & \cdots & 0 \\ \frac{s(2,0)}{2!} & \frac{s(2,1)}{2!} & \frac{s(2,2)}{2!} & \cdots & 0 \\ \vdots & \vdots & \vdots & \ddots & \vdots \\ \frac{s(N,0)}{N!} & \frac{s(N,1)}{N!} & \frac{s(N,2)}{N!} & \cdots & \frac{s(N,N)}{N!}\end{bmatrix}}_{\boldsymbol{S}_1^T}\underbrace{\begin{bmatrix}1 \\ x \\ x^2 \\ \vdots \\ x^N\end{bmatrix}}_{\boldsymbol{X}^T(x)},$$

hence, a transitive matrix relation can be finalized as

$$\boldsymbol{\chi}^T(x)=\boldsymbol{S}_1^T\boldsymbol{X}^T(x)\Rightarrow\boldsymbol{\chi}(x)=\boldsymbol{X}(x)\boldsymbol{S}_1,$$

which completes the proof.

Now, after inserting the transitive matrix relation (4) into the matrix relation (3), the matrix relation of the solution form leads to

$$y_i(x)=\boldsymbol{X}(x)\boldsymbol{S}_1\boldsymbol{L}(\alpha)\boldsymbol{A}_i=\boldsymbol{X}(x)\boldsymbol{M}(\alpha)\boldsymbol{A}_i;\ \boldsymbol{M}(\alpha)=\boldsymbol{S}_1\boldsymbol{L}(\alpha),\ i=1,2. \quad (5)$$

To deploy the matrix relation (5) in Eq. (1), taking its differentiation of k-th order, we have

$$y_i^{(k)}(x)=\boldsymbol{X}(x)\boldsymbol{T}^k\boldsymbol{M}(\alpha)\boldsymbol{A}_i, \quad (6)$$

where

$$\boldsymbol{T}^k = \begin{bmatrix} 0 & 1 & 0 & \cdots & 0 \\ 0 & 0 & 2 & \cdots & 0 \\ \vdots & \vdots & \vdots & \ddots & \vdots \\ 0 & 0 & 0 & 0 & N \\ 0 & 0 & 0 & 0 & 0 \end{bmatrix}^k .$$

On the other hand, the matrix relation of the term with delay arguments in Eq. (1) can be expanded after substituting $x \to \alpha_{jk}x + \beta_{jk}$ into the matrix relation (5). So, we have

$$y_i^{(k)}\left(\alpha_{jk}x + \beta_{jk}\right) = \boldsymbol{X}(x)\boldsymbol{B}\left(\alpha_{jk}, \beta_{jk}\right)\boldsymbol{T}^k\boldsymbol{M}(\alpha)\boldsymbol{A}_i,\ i = 1,2, \tag{7}$$

where $\boldsymbol{B}\left(\alpha_{jk}, \beta_{jk}\right)$ is the binomial coefficient matrix obtained from the expansion of $\left(\alpha_{jk}x + \beta_{jk}\right)^N$ and is of the form (see (Gökmen and Sezer, 2013) for its earlier form)

$$\boldsymbol{B}\left(\alpha_{jk}, \beta_{jk}\right) = \begin{bmatrix} \binom{0}{0}\alpha_{jk}^0\beta_{jk}^0 & \binom{1}{0}\alpha_{jk}^0\beta_{jk}^1 & \binom{2}{0}\alpha_{jk}^0\beta_{jk}^2 & \cdots & \binom{N}{0}\alpha_{jk}^0\beta_{jk}^N \\ 0 & \binom{1}{1}\alpha_{jk}^1\beta_{jk}^0 & \binom{2}{1}\alpha_{jk}^1\beta_{jk}^1 & \cdots & \binom{N}{1}\alpha_{jk}^1\beta_{jk}^{N-1} \\ 0 & 0 & \binom{2}{2}\alpha_{jk}^2\beta_{jk}^0 & \cdots & \binom{N}{2}\alpha_{jk}^2\beta_{jk}^{N-2} \\ \vdots & \vdots & \vdots & \ddots & \vdots \\ 0 & 0 & 0 & 0 & \binom{N}{N}\alpha_{jk}^N\beta_{jk}^0 \end{bmatrix}.$$

Using the collaboration of the matrix relations (5)-(7), the matrix form of Eq. (1) can be written as

$$\sum_{k=0}^{1}\left(\boldsymbol{P}_k(x)\overline{\boldsymbol{X}}(x) + \boldsymbol{Q}_k(x)\overline{\boldsymbol{X}}(x)\overline{\boldsymbol{B}}(\alpha_k, \beta_k)\right)\overline{\boldsymbol{T}^k}\ \overline{\boldsymbol{M}}(\alpha)\boldsymbol{A} = \boldsymbol{G}(x),$$

where

$$\boldsymbol{P}_k(x) = \begin{bmatrix} P_{11}^k(x) & P_{12}^k(x) \\ P_{21}^k(x) & P_{22}^k(x) \end{bmatrix},\ \overline{\boldsymbol{X}}(x) = \begin{bmatrix} \boldsymbol{X}(x) & 0 \\ 0 & \boldsymbol{X}(x) \end{bmatrix},\ \boldsymbol{Q}_k(x) = \begin{bmatrix} Q_{11}^k(x) & Q_{12}^k(x) \\ Q_{21}^k(x) & Q_{22}^k(x) \end{bmatrix},$$

$$\overline{\boldsymbol{B}}(\alpha_k, \beta_k) = \begin{bmatrix} \boldsymbol{B}(\alpha_{1k}, \beta_{1k}) & 0 \\ 0 & \boldsymbol{B}(\alpha_{2k}, \beta_{2k}) \end{bmatrix},\ \overline{\boldsymbol{T}^k} = \begin{bmatrix} \boldsymbol{T}^k & 0 \\ 0 & \boldsymbol{T}^k \end{bmatrix},\ \overline{\boldsymbol{M}}(\alpha) = \begin{bmatrix} \boldsymbol{M}(\alpha) & 0 \\ 0 & \boldsymbol{M}(\alpha) \end{bmatrix},$$

$$\boldsymbol{G}(x) = \begin{bmatrix} g_1(x) \\ g_2(x) \end{bmatrix},\ \boldsymbol{A} = \begin{bmatrix} \boldsymbol{A}_1 \\ \boldsymbol{A}_2 \end{bmatrix} = \begin{bmatrix} a_{10} & a_{11} & \cdots & a_{1N} & a_{20} & a_{21} & \cdots & a_{2N} \end{bmatrix}^T,$$

and with the collocation points $x_i = (b-a)i/N$, it admits the fundamental matrix equation

$$\boldsymbol{W}(\alpha)\boldsymbol{A} = \boldsymbol{G}, \tag{8}$$

where

$$\boldsymbol{W}(\alpha)=\sum_{k=0}^{1}\left(\boldsymbol{P}_k\overline{\boldsymbol{X}}+\boldsymbol{Q}_k\overline{\boldsymbol{X}}\ \overline{\boldsymbol{B}}(\alpha_k,\beta_k)\right)\overline{\boldsymbol{T}^k}\ \overline{\boldsymbol{M}}(\alpha),$$

such that

$$\boldsymbol{P}_k=\operatorname{diag}\left[\boldsymbol{P}_k(x_i)\right],\ \overline{\boldsymbol{X}}=\left[\ \overline{\boldsymbol{X}}(x_0)\quad \overline{\boldsymbol{X}}(x_1)\quad \cdots\quad \overline{\boldsymbol{X}}(x_N)\right]^T,\ \boldsymbol{Q}_k=\operatorname{diag}\left[\boldsymbol{Q}_k(x_i)\right],$$

and

$$\boldsymbol{G}=\left[\boldsymbol{G}(x_0)\quad \boldsymbol{G}(x_1)\quad \cdots\quad \boldsymbol{G}(x_N)\right]^T.$$

In addition, in view of the matrix relation (5), the matrix forms of the initial conditions of Eq. (1) are established as

$$\left.\begin{aligned} y_1(a)=\boldsymbol{X}(a)\boldsymbol{M}(\alpha)\boldsymbol{A}_1=\lambda_1\\ y_2(a)=\boldsymbol{X}(a)\boldsymbol{M}(\alpha)\boldsymbol{A}_2=\lambda_2\end{aligned}\right\}\Rightarrow\begin{bmatrix}\boldsymbol{U}_1(\alpha) & : & \lambda_1\\ \boldsymbol{U}_2(\alpha) & : & \lambda_2\end{bmatrix}. \tag{9}$$

Now, the conditional row matrices (9) are replaced by the proper rows related to $\boldsymbol{A}_1$ and $\boldsymbol{A}_2$ in Eq. (8). Then, the augmented matrix system is obtained as

$$\boldsymbol{W}(\alpha)\boldsymbol{A}=\boldsymbol{G}\Rightarrow\left[\boldsymbol{W}(\alpha)\quad :\quad \boldsymbol{G}\right]. \tag{10}$$

The matrix system (10) is solved after the parameter α is determined numerically. So, the unknown Charlier coefficients is thus, obtained and as a final step, the Charlier series solution is constructed when these coefficients are substituted into $\boldsymbol{A}_i$.

4. Numerical Examples

In this section, two illustrative examples are included to test the accuracy and efficiency of the method. In that case, a computer program on Mathematica 11.3 is developed in accordance with the mainframe of the method. Therefore, the computation results of the examples are directly overviewed and compared in tables and figures.

Example 4.1. Consider a system of first order delay differential equations

$$\left.\begin{aligned} y_1'(x)-xe^{x-1}y_2(x-1)=e^x-x\\ y_2'(x)+2x^2e^{-x-1}y_1(x+1)=2x^2-e^{-x}\end{aligned}\right\},\ 0\le x\le 1,$$

subject to its initial conditions $y_1(0)=y_2(0)=1$. Here, the exact solutions of the system are of the form $y_1(x)=e^x$ and $y_2(x)=e^{-x}$. This system is solved, by the time the present method is deployed for different *N*. Thus, the Charlier series solutions are demonstrated in Figure 1, where these solutions are in good agreement with the corresponding exact solutions. This consistency can be noticed via different *N* and the parameter α in Tables 1 and 2, taking approximately eleven decimal places of accuracy. In addition, Tables 1 and 2 reveal that the CPU timing cost of all computations remains low amount in terms of both *N*=4 and *N*=10.

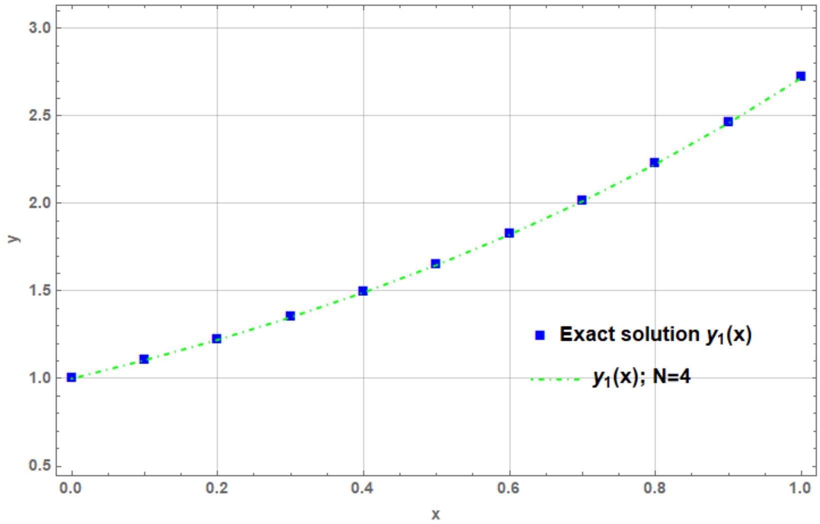

(a) Exact solution and Charlier series solution $y_1(x)$ for $\alpha = 0.1$

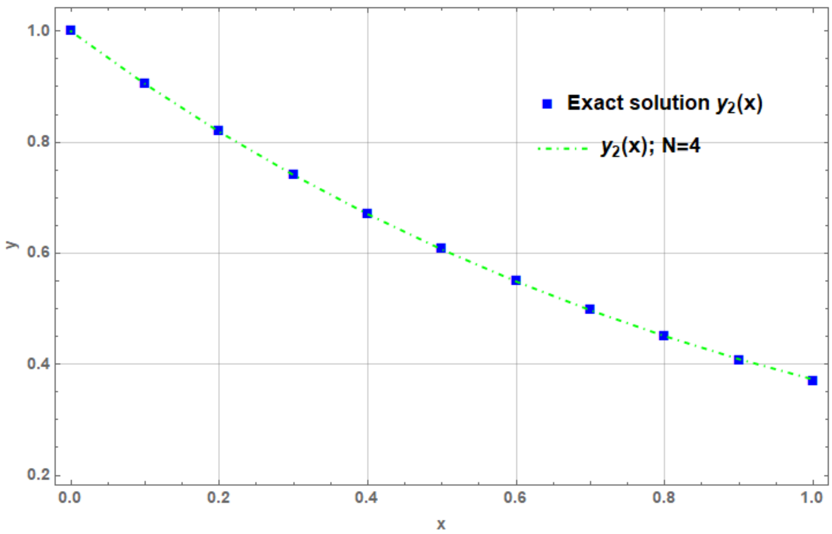

(b) Exact solution and Charlier series solution $y_2(x)$ for $\alpha = 0.1$

Figure 1. Displacements of the solutions for Example 4.1

Table 1. Comparison of CPU timing and the absolute errors with respect to the Charlier series solutions $\{y_1(x), y_2(x)\}$ with $\alpha = 0.1$ and N for Example 4.1

x_i	$\lvert e_1(x_i)\rvert$ $N=4$	$\lvert e_2(x_i)\rvert$ $N=4$	$\lvert e_1(x_i)\rvert$ $N=10$	$\lvert e_2(x_i)\rvert$ $N=10$
0.2	6.3298 e–05	1.0146 e–05	2.6489 e–011	2.5502 e–013
0.4	3.2572 e–05	3.3047 e–05	6.9767 e–011	2.3063 e–011
0.6	2.5548 e–04	2.7693 e–04	8.9304 e–011	7.3378 e–010
0.8	3.1847 e–04	1.4273 e–03	9.2578 e–011	1.0343 e–008
1.0	2.1181 e–04	4.8428 e–03	9.2488 e–011	8.7615 e–008
Time	0.0469		0.5313	

Table 2. Comparison of CPU timing and the absolute errors with respect to the Charlier series solutions $\{y_1(x),\ y_2(x)\}$ with $\alpha=1$ and N for Example 4.1

x_i	$\lvert e_1(x_i)\rvert$ $N=4$	$\lvert e_2(x_i)\rvert$ $N=4$	$\lvert e_1(x_i)\rvert$ $N=10$	$\lvert e_2(x_i)\rvert$ $N=10$
0.2	6.3298 e–05	1.0146 e–05	3.7095 e–011	2.9066 e–013
0.4	3.2572 e–05	3.3047 e–05	8.8780 e–011	2.3332 e–011
0.6	2.5548 e–04	2.7693 e–04	1.1056 e–010	7.3501 e–010
0.8	3.1847 e–04	1.4273 e–03	1.1412 e–010	1.0350 e–008
1.0	2.1181 e–04	4.8428 e–03	1.1405 e–010	8.7658 e–008
Time	0.0313		0.4219	

Example 4.2. Consider a system of first order delay differential equations

$$\left.\begin{aligned} &y_1'(x)+x^2y_2'(0.5x-0.1)+xy_1(x)=e^x+e^xx+x^2\cos(0.5x-0.1)\\ &y_2'(x)-\cos(x)y_1'(0.5x+0.5)+y_2(x)=\cos(x)-e^{0.5x+0.5}\cos(x)+\sin(x)\end{aligned}\right\},\ -1\le x\le b,$$

subject to its initial conditions $y_1(-1)=\exp(-1)$ and $y_2(-1)=-\sin(1)$. Here, the exact solutions of this system are of the form $y_1(x)=e^x$ and $y_2(x)=\sin(x)$. After solving this system with the aid of the present method for b={1,3}, the Charlier series solutions are illustrated in Figure 2, respectively. In addition, these solutions can be simulated on both normal (b=1) and long spatial (b=3) intervals, as in Figures 2 and 3, respectively. The clear approaches to the exact solutions on both figures are determined. Table 3 approves these precisions in numerical aspect and demonstrates the low CPU timing results even for higher computation limit.

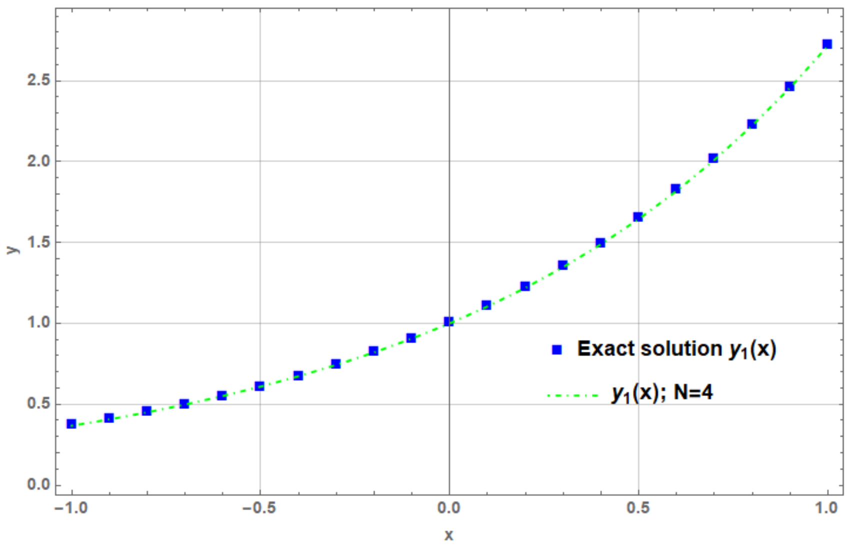

(a) Exact solution and Charlier series solution $y_1(x)$ for $\alpha=0.1$

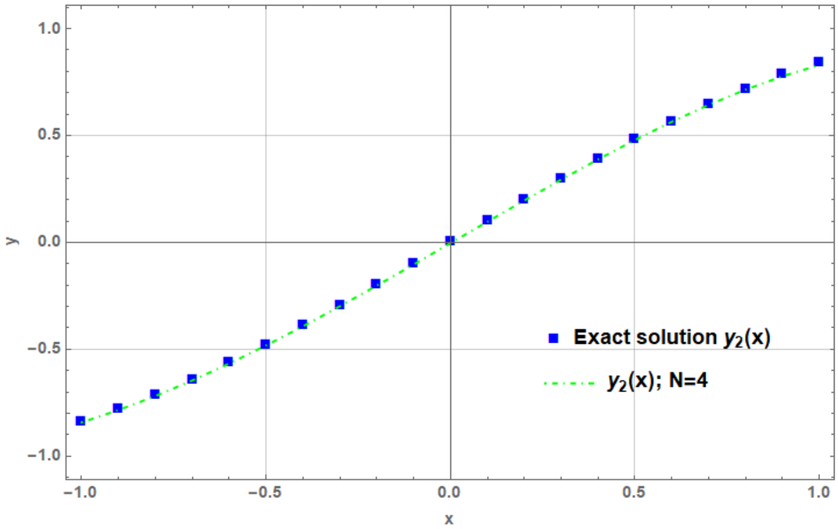

(b) Exact solution and Charlier series solution $y_2(x)$ for $\alpha = 0.1$

Figure 2. Displacements of the solutions for Example 4.2

Table 3. Comparison of CPU timing and the absolute errors with respect to the Charlier series solutions $\{y_1(x),\ y_2(x)\}$ with $\alpha = 0.1$ and N for Example 4.2

x_i	$\lvert e_1(x_i)\rvert$ $N=4$	$\lvert e_2(x_i)\rvert$ $N=4$	$\lvert e_1(x_i)\rvert$ $N=10$	$\lvert e_2(x_i)\rvert$ $N=10$
–0.6	2.9193 e–03	1.6008 e–03	3.5522 e–010	3.5888 e–011
–0.2	2.6760 e–03	2.9928 e–03	4.3578 e–010	1.0054 e–010
0.2	7.2685 e–04	1.9825 e–03	5.3109 e–010	1.0237 e–010
0.6	1.9825 e–03	1.1841 e–04	4.6041 e–010	1.9166 e–010
1.0	1.0676 e–03	1.1410 e–02	6.7767 e–010	5.9516 e–009
Time	0.0469		0.4063	

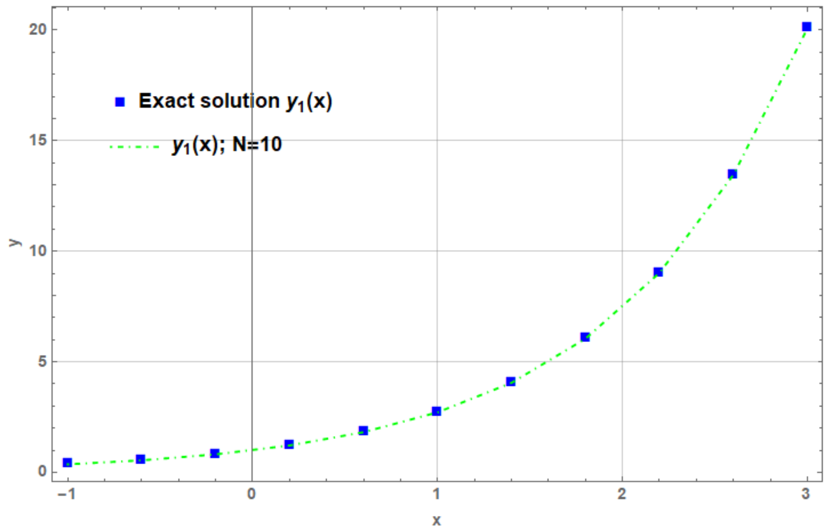

(a) Exact solution and Charlier series solution $y_1(x)$ for $\alpha = 0.1$.

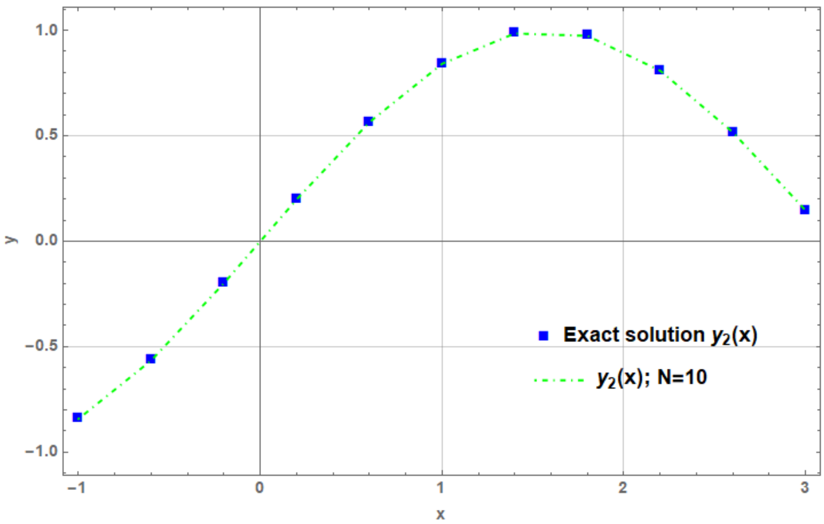

(b) Exact solution and Charlier series solution $y_2(x)$ for $\alpha = 0.1$.

Figure 3. Displacements of the solutions on [-1,3] for Example 4.2.

5. Conclusions

SDDEs have been suitably solved by the present method based on the Charlier polynomials and the collaboration of the matrices of the terms in the system (1). In that case, a computer program of the method has managed to perform its routines on a considered example. Thus, the numerical and graphical investigations have revealed the applicability and practicability of the present method, as can be seen in Figures 1-3 and Tables 1-3. Although SDDEs have the complicated terms in virtue of the delay arguments, the present method solves two examples immediately, as noticed in Tables 1 and 3. In addition, Tables 1 and 2 show that the parameter-α has played a key role in the accuracy for its different values. The present method sheds light on new aspect and advancement regarding the use of the combinatorial polynomials in SDDEs. Thereby, one can admit that the present method is inventive and straightforward to employ the systems of integro-differential-delay and nonlinear differential-delay equations, of course, some modifications can be implemented.

Author Statement

The authors confirm contribution to the paper as follows: study conception and design: M. Sezer, Ö.K. Kürkçü; data collection: Ö.K. Kürkçü; analysis and interpretation of results: M. Sezer, Ö.K. Kürkçü; draft manuscript preparation: Ö.K. Kürkçü. All authors reviewed the results and approved the final version of the manuscript.

Conflict of Interest

The authors declare no conflict of interest.

References

Abdel-Halim Hassan, I.H. (2008). Application to differential transformation method for solving systems of differential equations. *Applied Mathematical Modelling*, *32*(12), 2552–2559.

Akyüz, A., & Sezer, M. (2003). Chebyshev polynomial solutions of systems of high-order linear differential equations with variable coefficients. *Applied Mathematics and Computation, 144*, 237–247.

Butzer, P.L., Hauss, M., & Schmidt, M. (1989). Factorial functions and Stirling numbers of fractional orders. *Results in Mathematics, 16*, 16–48.

Culshaw, R.V., & Ruan, S. (2000). A delay-differential equation model of HIV infection of $CD4^+$ T-cells. *Mathematical Biosciences*, *165*(1), 27–39.

Cushing, J.M. (1977). *Integro differential Equations and Delay Models in Population Dynamics*. Heidelberg: Springer-Verlag.

Deniz, S. (2021). Semi-analytical approach for solving a model for HIV infection of CD4+ T-cells. *TWMS Journal of Applied and Engineering Mathematics*, *11*(1), 273-281.

Dunster, T.M. (2001). Uniform asymptotic expansions for Charlier polynomials. *Journal of Approximation Theory*, *112*, 93-133.

Gokmen, E., Isik, O.R., & Sezer, M. (2015). Taylor collocation approach for delayed Lotka–Volterra predator–prey system. *Applied Mathematics and Computation*, *268*, 671–684.

Gökmen, E., & Sezer, M. (2013). Taylor collocation method for systems of high-order linear differential–difference equations with variable coefficients. *Ain Shams Engineering Journal*, *4*, 117–125.

Huang, X.-M., Lin, Y., & Zhao, Y.-Q. (2021). Asymptotics of the Charlier polynomials via difference equation methods. *Analysis and Applications*, *19*(04), 679-713.

Kuang, Y. (1993). *Delay Differential Equations with Applications in Population Dynamics*. New York: Academic Press.

Pamuk, S. (2005). The decomposition method for continuous population models for single and interacting species. *Applied Mathematics and Computation, 163*, 79-88.

Roman, S. (1984). *The umbral calculus*. New York: Academic Press.

Srivastava, H.M., & Deniz, S. (2021). A new modified semi-analytical technique for a fractional-order Ebola virus disease model. *RACSAM 115*, 137. DOI:10.1007/s13398-021-01081-9.

Szegö, G. (1975). *Orthogonal polynomials*. Providence Rhode Island: American Mathematical Society.

Tatari, M., & Dehghan, M. (2009). Improvement of He's variational iteration method for solving systems of differential equations. *Computers & Mathematics with Applications*, *58*(11-12), 2160–2166.

Thirumalai, S., Seshadri, R., & Yuzbasi, S. (2021). Spectral solutions of fractional differential equations modelling combined drug therapy for HIV infection. *Chaos, Solitons and Fractals, 151*, 111234.

Varma, S., & Taşdelen, F. (2012). Szász type operators involving Charlier polynomials. *Mathematical and Computer Modelling, 56*, 118–122.

Yüzbaşı, Ş., & Karaçayır, M. (2017). An exponential Galerkin method for solutions of HIV infection model of CD 4+ T-cells. *Computational Biology and Chemistry*, *67*, 205–212.

Scientific Research Communications

Research Article

Sci. Res. Comm. (2022)
Volume 2, Issue 1
doi: 10.52460/src.2022.005

Prevalence of Hepatitis-B virus and HIV infections in Pregnant Women Receiving Antenatal Care Services, Kano – Nigeria

Sulaiman Danjuma Dausayi[1], Umar Muazu Yunusa[2,*], Isa Yunusa[3], Zulaiha Gidado Mukhtar[4], Anas Lawan Sulaiman[5], Fatima Sunusi Gaya[6]

[1] Disease Control and Epidemiology, Kano State Primary Health Care Management Board, Kano, Nigeria
[2] Division of Biochemistry, Graduate School of Natural and Applied Sciences, Dokuz Eylül University, Izmir, Turkey
[3] Kampala International University, Department of Biochemistry, Kampala, Uganda
[4] Department of Science Laboratory Technology, School of Technology, Kano State Polytechnic, Kano, Nigeria
[5] Department of Biochemistry, Kano University of Science and Technology, Wudil, Kano, Nigeria
[6] Bayero University Kano, College of Clinical Sciences, Department of Medicine and Surgery, Kano, Nigeria
* Corresponding author: umarmuazuyunusa@gmail.com

Received: 26.11.2021 Accepted: 29.01.2022

Abstract

The dreadful nature of hepatitis-B virus (HBV) and HIV infections and their common mode of transmission during pregnancy have made them become an important global health problem and a leading cause of maternal complications and neonatal deaths in both developed and developing countries. The current study determined the seroprevalence of HBV and HIV amongst pregnant women receiving antenatal care services in Kano state. Structured questionnaires were distributed to 276 (14-49 years) consenting pregnant women across the six selected health facilities to obtain demographic and socio-economic data. Three (3) ml of venous blood sample were drawn by venipuncture and centrifuged at 3000 rpm for 5 min. The serum was tested for the presence of HIV antibodies using the Abbott Determine HIV 1/2 test kit and HBV antibodies using a rapid diagnostic test kit (DiaSpot Diagnostics, USA). The $\chi 2$ test for independence was determined using GraphPad InStat software (version 3.0). Sociodemographic characteristics of the respondents showed 95.7% of the respondents as being married, 64.5% lived in a monogamous family, 62.4% petty traders, 26.8% unemployed, 57.4% of them are 21 – 30 years of age, 41.3% have Quranic education, 28.3% are 1st gravida while 36.9% have more than 4 children. Additionally, 1.4% of HIV and 8% of HBV cases were confirmed. The chi-squared test for independence ($\chi 2$=13.078, P=0.0003) showed a significant relationship between the two variables. HIV and HBV infections existed in the study group. Regular screening, awareness, and health education programs on the mode of their transmission should be directed to pregnant women to prevent vertical transmission.

Keywords: Pregnancy, HIV and Hepatitis-B virus infections

1. Introduction

Pregnancy is characterized as a period of reproduction during which a woman carries one or more offspring from the implantation of a fertilized zygote in the uterus throughout gestation (Mohamed et al., 2016). However, this exciting time is known to triggers endocrine, physiological, anatomical, biochemical, and immunological response; and to have a well-known effect in the T helper 1-T helper 2 balance towards a T helper 2 response, which increases the secretion of regulatory T cells and in turn depressed immune response thereby resulting in the successful infection and proliferation of viral DNA (Borgia et al., 2012; Costantine, 2014). Human immunodeficiency virus (HIV) and hepatitis B virus (HBV) infections pose a public health challenge causing about two billion infections worldwide (Adegbesan-Omilabu et al., 2015; Platt et al., 2016), with an approximate 350 million people remaining chronically infected (Schilsky, 2013). Out of these, about 50% acquired their infections either perinatally or in early childhood (Lavanchy, 2005). The appalling nature of both viral infections and their common route of transmission through blood and body fluids especially during unprotected heterosexual contact, mother to child transmission, and ability to cause chronic disease state in affected individuals account for their dual burden of co-morbidity during pregnancy (Kourtis et al., 2012).

HBV belong to a member of the hepadnaviridae family and envelops a partially double-stranded DNA virus has numerous antigenic components such as hepatitis B envelope antigen (HBeAg), hepatitis B core antigen (HBcAg) and hepatitis B surface antigen (HBsAg) (Mekonnen et al., 2018). Due to its vertical transmission nature, hepatitis B is associated with maternal complications, and death accompanied by impaired mental and physical health of the child (Ugbebor et al., 2011). This is followed by liver cirrhosis and hepatocellular carcinoma in young adults (Negero et al., 2011). Its high prevalence (>8% of the population) has been reported in Pacific Islands, South-East Asia, China, the Amazon basin, Sub-Saharan Africa and parts of the Middle-East with intermediated prevalence (2–7%) in Eastern and Southern Europe, Central and South America, South Asia, and Russia. On the other hand, the areas with low endemicity (<2%) include Australia, Western Europe, and the United States (Te and Jensen, 2010; World Health Organization, 2013). In Nigeria, different prevalence rate of HBV in pregnant women was reported in different localities amongst which are 7.3%, 8.2% and 16.3% documented by Adegbesan-Omilabu et al. (2015), Olokoba et al. (2011) and Adeyemi et al. (2014), respectively.

Since it was first discovered in 1981 in the United States (Gottlieb et al., 1981), AIDS which was caused by HIV has become a global pandemic (Perpetus et al., 2012) with highest number of people (63%) with the virus living in sub-Saharan Africa (Adeniran et al., 2014). With about 1.9 million people currently living with HIV in Nigeria, the country has a national prevalence rate of 1.4% (i.e., 1.9% women, versus 0.9% men) among adults aged 15–49 years (Federal Ministry of Health, UNAIDS, and National Agency for the Control of AIDS, 2019). Previous estimates had indicated a national HIV prevalence of 2.8% (about 3.1 million people) (AVERT global information and education on HIV and AIDS, 2018). Potential vertical transmission of this deadly virus (HIV) during the gestation period is a major concern, because of the attendant consequences of morbidity and mortality of these infections (Kourtis et al., 2012). The infection, if it happens, pre-exposes the children to common childhood diseases like measles, diarrhoea, common cold, etc. that can be used as markers of immune decline (Makokha et al., 2003). Thus, the present study aimed to determine the prevalence of HIV and HBV amongst pregnant women attending some antenatal care services in Kano state primary health care management board.

2. Materials and Method

2.1. Target Population

The study population included primi and multi-gravid pregnant women (14-49 years) attending antenatal services in six zones in Kano state primary health care management board. A total of 276 consented pregnant women were recruited for the study.

2.2. Sample Size Determination

By taking Adeyemi et al. (2014)'s 16.3% prevalence rate of HBV, the sample size was determined using the formula, $N = \frac{Z^2 p(1-p)}{d^2}$ (Bartlett et al., 2001) where

N = sample size

d = margin of error (5%)

p = prevalence of 16.3%

z = critical value at 95 % confidence level (1.96)

Substituting the above values in the given formula yields

$$N = \frac{(1.96)^2 \times 0.163(0.837)}{(0.05)^2} = 209.6$$

Therefore, a minimum sample size of 210 is obtained. Adjusting for attrition, the sample size was rounded up to 276 pregnant women.

2.3. Sampling Technique

Six hospitals (one from each zone) were randomly selected using systematic sampling. The number of consenting respondents in each hospital was 46 (totaling 276). Respondents were randomly recruited through systematic sampling for the study on different clinic days.

2.4. Data Collection

A structured questionnaire was designed and administered to consented pregnant women. The questionnaire contained some socio-demographic and economic characteristics of the participants. Figure 1 shows respondent filling the questionnaire.

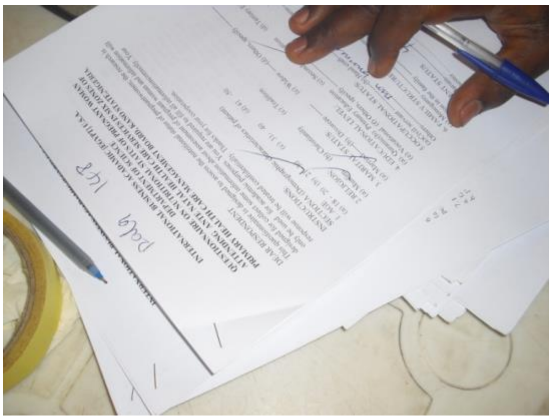

Figure 1. A respondent filling the questionnaire

2.5. Informed Consent and Ethical Issues

Informed consents were obtained from the respondents before sample collection and all data were kept confidential in accordance with world medical association ethical principle for medical research involving human subjects (World Medical Association, 2013). Ethical clearance was sought and obtained from Kano state ministry of health prior to commencement of the study.

2.6. Assay

A 3 ml venous blood sample was drawn by venipuncture (Figure 2) from women and collected in a labelled plain universal specimen bottle. Each clotted sample was centrifuged at 3000 rpm for 5 min. The serum was subsequently separated from each blood sample and stored frozen (-20 °C) until further analysis. Each pregnant woman's serum was tested for the presence of HIV antibodies using Abbott Determine HIV 1/2 test kit (Abbot Laboratories, Illinois, USA) and HBV antibodies using rapid diagnostic tests (DiaSpot Diagnostics, USA). The standard operating procedures (SOPs) of each of the manufacturers were strictly followed.

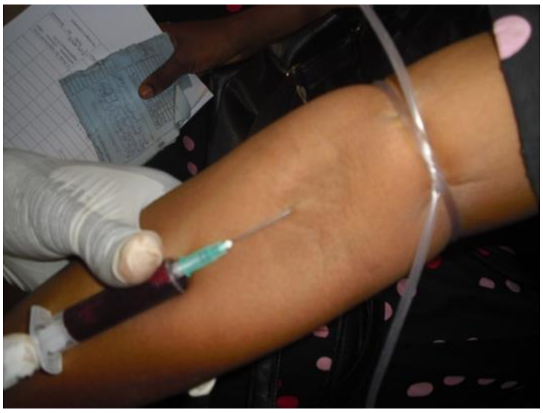

Figure 2. Blood sample being drawn by venipuncture

2.7. Data Analysis

The data retrieved were analyzed and depicted in the tables using percentages and proportions to compute the socio-demographic and economic variables. A chi-squared test for independence was used for inferential statistics to determine the possible relationship among the variables of the study.

3. Results

The economic and demographic characteristics of the respondents are presented in Table 1. The majority of the respondents have Quranic education (41.3%); 2.2% studied up to the advanced level, 62.4% are petty traders and 26.8% are unemployed. Likewise, 57.4% (representing the majority) of the respondents are in the range of 21 – 30 years of age, minority (8%) are in between 41 – 50 years of age, 95.7% are married, and 64.5% are living in a monogamous family, 36.9% have more than 4 children and 28.3% are 1st gravida mothers.

Table 1. Socio-demographic features of the population under study

Variables	N (276)	Percentage (%)
Employment type		
Civil servant	10	3.6
Handcraft	18	6.5
Trading	172	62.4
Unemployed	74	26.8
Others	2	0.7
Family type		
Monogamy	178	64.5
Polygamy	98	36.5
Marital status		
Married	264	95.7
Divorced	8	2.9
Widow	4	1.4
Religion		
Islam	274	99.3
Christianity	02	0.7
Educational level		
Quranic	114	41.3
Primary	48	17.4
Secondary	106	38.4
Tertiary	6	2.2
Vocational	2	0.7
Age (years)		
11-20	62	22.5
21-30	142	57.4
31-40	50	18.1
41-50	22	8.0
Gravidarum		
1	78	28.3
2	44	15.9
3	22	8.0
4	30	10.9
4+	102	36.9

Table 2 presents the infectious status of pregnant women. Out of 276 consented pregnant women 4 are HIV seropositive giving a prevalence of 1.4%. Likewise, 22 out of 276 study participants (8%) are also seropositive for HBV test. All in all, the number of respondents with HBV infections are higher than that of HIV. The chi-squared test for independence (13.078) showed the two variables to be significantly associated with each other (P=0.0003) and each infection had a significant relationship with the other group.

Table 2. Infectious status of a pregnant woman

Parameter	Reactive		Non-reactive	
	N (276)	Percentage (%)	N (276)	Percentage (%)
HIV	4	1.4	272	98.6
HBV	22	8	254	92

Chi-square: 13.078; The P value is 0.0003

The row and column variables are significantly associated.

4. Discussion

Viral diseases such as HIV and HBV are life-threatening diseases that have become an important public health issue in both developed and developing countries. The problem tends to be more profound in sub-Saharan Africa including Nigeria. During pregnancy, HIV and HBV screening is important to initiate early antiretroviral therapy (ART) that improves maternal health and prevent the risk of vertical transmission (mother to child) of retroviral diseases (Günthard et al., 2016). Taking this into consideration, the present study investigated the prevalence of HIV and HBV amongst pregnant women in the study area. Results presented from the present study in Table 2 showed the prevalence of HBV infection as 8%. This value is similar to 7.9% (Jatau et al., 2009; Yakasai et al., 2012), 8.2% (Olokoba et al., 2011), 8.3% (Luka et al., 2008; Anaedobe et al., 2015) but quite differ with 2.2% (Mbamara and Obiechina, 2010), 4.89% (Caroline et al., 2016), 7.3% (Adegbesan-Omilabu et al., 2015), 12% (Mbaawuaga et al., 2014; Musa et al., 2015), 16.3% (Adeyemi et al., 2014) prevalence figures documented in various studies and in various locations in Nigeria. This level of endemicity is worrisome considering the consequences both for the mother's health and that of her baby. Without treatment, HBV infection can progress chronically and may be clinically asymptomatic, or may progress to cause liver cancer or liver damage that leads to liver failure (Molla et al., 2015). It can also progress to attack and damage ovarian follicle or placental capillary endothelium (Yu et al., 2013).

The 1.4% HIV prevalence obtained in the current study is the same as the 2019 national HIV prevalence rate of 1.4% reported by the federal ministry of health (FMoH), UNAIDS and national agency for the control of AIDS (NACA) among women of reproductive ages (15–49 years) living in Nigeria (Federal Ministry of Health et al., 2019). However, this value is lower than 2.8% of previous national estimates (AVERT global information and education on HIV and AIDS, 2018); and 3.0% (Okerentugba et al., 2015), 3.2% (Isichei et al., 2015), 4.9% (Ibrahim et al., 2013), 5.9% (Caroline et al., 2016); but higher than 0.95% (Ajoge et al., 2008) previously reported in various localities in Nigeria. The low HIV prevalence observed in the present study could be explained by the effort of various government and non-governmental agencies programs in the country in raising awareness about the importance of HIV screening and its prevention. Pregnant women infected with HIV have an increased risk of anemia, hypertensive disease, hemorrhage due to thrombocytopenia (Caroline et al., 2016), eight times higher mortality rate and three times the risk of puerperal sepsis in comparison with non-infected negative women (Calvert and Ronsmans, 2013; Zaba et al., 2013). These consequences tend to progress to their offspring, immediate family, health workers, social and economic structure (Egesie and Mbooh, 2008). In general, this prospective cohort study shows HBV infections as having a higher prevalence than HIV. Hepatitis B and human immunodeficiency viruses tests during gestation benefit the women in the reinforcement of safe sex practices, provision of opportunity for counselling on infant feeding options, and enabling a woman to make informed choices about future pregnancies.

5. Conclusion

The findings of the present study conclude that viral infections of hepatitis and human immunodeficiency does exist amongst the study group with HBV having a higher endemicity of 8%. To decrease the prevalence of these viral infections, we recommend that all pregnant women should be screened for HIV and HBV, and health education programs on the mode of their transmission to prevent mother-to-child transmission should be instituted in all antenatal care clinics to raise the awareness to mothers.

Author Statement

The authors confirm contribution to the paper as follows: study conception and design: Sulaiman Danjuma Dausayi, Isa Yunusa; data collection: Sulaiman Danjuma Dausayi, Fatima Sunusi Gaya, Anas Lawan Sulaiman; analysis and interpretation of results: Umar Muazu Yunusa, Isa Yunusa, Zulaiha Gidado Mukhtar; draft manuscript preparation: Umar Muazu Yunusa, Zulaiha Gidado Mukhtar. All authors reviewed the results and approved the final version of the manuscript.

Conflict of Interest

The authors declare no conflict of interest.

References

Adegbesan-Omilabu, M. A., Okunade, K. S., Gbadegesin, A., Olowoselu, O. F., Oluwole, A. A., & Omilabu, S. A. (2015). Seroprevalence of hepatitis B virus infection among pregnant women at the antenatal booking clinic of a Tertiary Hospital in Lagos Nigeria. *Nigerian Journal of Clinical Practice*, *18*(6), 819-823.

Adeniran, A. S., Raji, S. T., Saidu, R., & Omokanye, L. O. (2014). Partner disclosure and human immunodeficiency virus serology status among antenatal clinic attendees with human immunodeficiency virus infection in Ilorin. *Journal of Medical Investigations and Practice, 9*(3) 112-115.

Adeyemi, A. B., Enabor, O. O., Ugwu, I. A., Abraham, O. A., Bello, F. A., & Olayemi, O. (2014). Prevalence of antenatal hepatitis B infection in tertiary and non-tertiary health facilities in Ibadan, Nigeria. *Nigerian journal of medicine: journal of the National Association of Resident Doctors of Nigeria*, *23*(3), 248-253.

Ajoge, H. O., Ahmad, A. A., Olonitola, O. S., Abdulsalam, A., Onujabe, M. I., Muktar, H. M., & Shittu, S. O. (2008). The prevalence of human immunodeficiency virus infection among pregnant women in rural settlements of Ebira-land. *International Journal of Biological and Chemical Sciences*, *2*(1).

Anaedobe, C. G., Fowotade, A., Omoruyi, C. E., & Bakare, R. A. (2015). Prevalence, socio-demographic features and risk factors of Hepatitis B virus infection among pregnant women in Southwestern Nigeria. *The Pan African Medical Journal*, *20*(406), 1-11.

AVERT. Global information and education on HIV and AIDS. HIV and Aids in Nigeria. 2018. Available: https://www.avert.org/professionals/hiv-around-world/sub-saharan-africa/nigeria#footnote2_cisibwc. [Accessed: July 8, 2019].

Bartlett, J. E., Kotrlik, J. W., Higgins, C. C. (2001). Organizational research: Determining appropriate sample size in survey research. *Information Technology, Learning, and Performance Journal*, *19*(1), 43-50.

Borgia, G., Carleo, M. A., Gaeta, G. B., & Gentile, I. (2012). Hepatitis B in pregnancy. *World journal of gastroenterology: WJG*, *18*(34), 4677.

Calvert, C., & Ronsmans, C. (2013). HIV and the risk of direct obstetric complications: a systematic review and meta-analysis. *PloS one*, *8*(10), e74848.

Caroline, I., Hannah, O., & Adaunwo, O. D. (2016). A Retrospective Study of the Seroprevalence of Antibodies to HbsAg, HIV-1/2 And Syphilis Amongst Pregnant Women At Booking In A Tertiary Hospital In Port Harcourt, Southern Nigeria. *IOSR Journal of Dental and Medical Sciences, 15*(6), 86-92.

Costantine, M. (2014). Physiologic and pharmacokinetic changes in pregnancy. *Frontiers in Pharmacology*, *5*, 65.

Egesie, U., & Mbooh, T. (2008). Seroprevalence of human immunodeficiency virus (hiv) infection in pregnant women in amassoma, nigeria. *African Journal of Biomedical Research*, *11*(1), 111-113.

Federal Ministry of Health, UNAIDS, and National Agency for the Control of AIDS (NACA). New survey results indicate that Nigeria has an HIV prevalence of 1.4% 2030 - End. AIDS epidemic. 2019. Available: https://www.unaids.org/en/resources/presscentre/pressreleaseandstatementarchive/2019/march/20190314_nigeria. [Accessed: July 8, 2019].

Gottlieb, M. S., Schroff, R., Schanker, H. M., Weisman, J. D., Fan, P. T., Wolf, R. A., & Saxon, A. (1981). Pneumocystis carinii pneumonia and mucosal candidiasis in previously healthy homosexual men: evidence of a new acquired cellular immunodeficiency. *New England Journal of Medicine*, *305*(24), 1425-1431.

Günthard, H. F., Saag, M. S., Benson, C. A., Del Rio, C., Eron, J. J., Gallant, J. E., et al. (2016). Antiretroviral drugs for treatment and prevention of HIV infection in adults: 2016 recommendations of the International Antiviral Society–USA panel. *Jama*, *316*(2), 191-210.

Ibrahim, I. A., Owoeye, G. I., & Obilahi, A. (2013). The burden of HIV infection among women attending antenatal clinic in a semi-urban Nigerian town. *West Indian Medical Journal*, *62*(4), 323-328.

Isichei, C., Brown, P., Isichei, M., Njab, J., Oyebode, T., & Okonkwo, P. (2015). Hiv Prevalence and Associated Risk Factors Among Rural Pregnant Women in North Central Nigeria. *Am. J. Heal. Res.*, *3*(1), 18-23.

Jatau, E. D., & Yabaya, A. (2009). Sero prevalance of Hepatisis B Virus in pregnant women attending a clinic in Zaria, Nigeria. *Science World Journal*, *4*(2), 7-9.

Bartlett, J. E., Kotrlik, J. W., Higgins, C. C. (2001). Organizational research: Determining appropriate sample size in survey research. *Information Technology, Learning, and Performance Journal*, *19*(1), 43-50.

Kourtis, A. P., Bulterys, M., Hu, D. J., & Jamieson, D. J. (2012). HIV–HBV coinfection—A global challenge. *New England Journal of Medicine*, *366*(19), 1749-1752.

Lavanchy, D. (2005). Worldwide epidemiology of HBV infection, disease burden, and vaccine prevention. *Journal of Clinical Virology*, *34*, S1-S3.

Luka, S. A., Ibrahim, M. B., & Iliya, S. N. (2008). Sero-prevalence of hepatitis B surface antigen among pregnant women attending Ahmadu Bello University Teaching Hospital, Zaria, Nigeria. *Nigerian Journal of Parasitology*, *29*(1), 38-41.

Makokha, E. P., Ogolla, M., Orago, A. S. S., Koech, D. K., Mpoke, S., Esamai, F., ... & Tukei, P. M. (2003). CD4T Lymphocyte subsets and disease manifestation in children with and without HIV born to HIV-1 infected mothers. *East African Medical Journal*, *80*(2), 95-100.

Mbaawuaga, E. M., Iroegbu, C. U., Ike, A. C., & Jombo, G. T. A. (2014). Studies on prevalence, co-infection and associated risk factors of hepatitis B virus (HBV) and Human immunodeficiency virus (HIV) in Benue State, Nigeria. *Science Journal of Public Health*, *2*(6), 569-576.

Mbamara, S. U., & Obiechina, N. J. A. (2010). Seroprevalence of hepatitis B surface antigen among antenatal clinic attendees in a private specialist hospital in Onitsha, Southeast Nigeria. *Nigerian Medical Journal*, *51*(4), 152.

Mekonnen, R., Admasu, D., & Belete, M. (2018). Sero-Prevalence of Hepatitis B Virus and associated factors among pregnant mothers attending antenatal care in Public Health Facilities, Dire Dawa. *Journal of Medical Microbiology & Diagnosis*, *7*(3), 1-8.

Mohamed, A. O., Hamza, K. M., & Babker, A. M. (2016). Physiological changes in some hematological and coagulation profile among Sudanese healthy pregnant women. *International Journal of Medical Science and Public Health*, *5*(3), 525-528.

Molla, S., Munshea, A., & Nibret, E. (2015). Seroprevalence of hepatitis B surface antigen and anti HCV antibody and its associated risk factors among pregnant women attending maternity ward of Felege Hiwot Referral Hospital, northwest Ethiopia: a cross-sectional study. *Virology Journal*, *12*(1), 1-9.

Musa, B. M., Bussell, S., Borodo, M. M., Samaila, A. A., & Femi, O. L. (2015). Prevalence of hepatitis B virus infection in Nigeria, 2000-2013: a systematic review and meta-analysis. *Nigerian Journal of Clinical Practice*, *18*(2), 163-172.

Negero, A., Sisay, Z., & Medhin, G. (2011). Prevalence of Hepatitis B surface antigen (HBsAg) among visitors of Shashemene General Hospital voluntary counseling and testing center. *BMC Research Notes*, *4*(1), 1-5.

Okerentugba, P. O., Uchendu, S. C., & Okonko, I. O. (2015). Prevalence of HIV among pregnant women in Rumubiakani, Port Harcourt, Nigeria. *Public Health Research*, *5*(2), 58-65.

Olokoba, A. B., Salawu, F. K., Damburam, A., Olokoba, L. B., Midala, J. K., Badung, H. L., & Olatinwo, A. W. O. (2011). Hepatitis B virus infection amongst pregnant women in north-eastern-a call for action. *Nigerian Journal of Clinical Practice*, *14*(1), 10-13.

Perpetus, C. I., Fidelis, A. O., Joseph, A., & Paul, O. E. (2012). Human immunodeficiency virus (HIV) seroprevalence and pregnancy outcome among obstetric population in Abakaliki, Southeast Nigeria. *Journal of Public Health and Epidemiology*, *4*(10), 290-293.

Platt, L., Easterbrook, P., Gower, E., McDonald, B., Sabin, K., McGowan, C., ... & Vickerman, P. (2016). Prevalence and burden of HCV co-infection in people living with HIV: a global systematic review and meta-analysis. *The Lancet Infectious Diseases*, *16*(7), 797-808.

Schilsky, M. L. (2013, April). Hepatitis B “360”. In *Transplantation Proceedings* (Vol. 45, No. 3, 982-985). Elsevier.

Te, H. S., & Jensen, D. M. (2010). Epidemiology of hepatitis B and C viruses: a global overview. *Clinics in Liver Disease*, *14*(1), 1-21.

Ugbebor, O., Aigbirior, M., Osazuwa, F., Enabudoso, E., & Zabayo, O. (2011). The prevalence of hepatitis B and C viral infections among pregnant women. *North American Journal of Medical Sciences*, *3*(5), 238-241.

World Health Organization. (2013). Global policy report on the prevention and control of viral hepatitis in WHO Member States. 1-220.

World Medical Association. (2013). Declaration of Helsinki: ethical principles for medical research involving human subjects. *JAMA, 310*(20): 2191–2194.

Yakasai, I. A., Ayyuba, R. U., Abubakar, I. S., & Ibrahim, S. A. (2012). Sero-prevalence of hepatitis B virus infection and its risk factors among pregnant women attending antenatal clinic at Aminu Kano Teaching Hospital, Kano, Nigeria. *Journal of Basic and Clinical Reproductive Sciences*, *1*(1-2), 49-55.

Yu, M., Jiang, Q., Gu, X., Ju, L., Ji, Y., Wu, K., & Jiang, H. (2013). Correlation between vertical transmission of hepatitis B virus and the expression of HBsAg in ovarian follicles and placenta. *PloS one*, *8*(1), e54246.

Zaba, B., Calvert, C., Marston, M., Isingo, R., Nakiyingi-Miiro, J., Lutalo, T., ... & Ronsmans, C. (2013). Effect of HIV infection on pregnancy-related mortality in sub-Saharan Africa: secondary analyses of pooled community-based data from the network for Analysing Longitudinal Population-based HIV/AIDS data on Africa (ALPHA). *The Lancet*, *381*(9879), 1763-1771.